DESCRIPTION OF A 30 cm-H_2-BUBBLE CHAMBER

J. REUSS

DESCRIPTION OF A 30 cm-H_2-BUBBLE CHAMBER

DESCRIPTION OF A 30 cm-H_2-BUBBLE CHAMBER

PROEFSCHRIFT

TER VERKRIJGING VAN DE GRAAD VAN DOCTOR IN DE WIS- EN NATUURKUNDE AAN DE RIJKSUNIVERSITEIT TE LEIDEN OP GEZAG VAN DE RECTOR MAGNIFICUS DR. G. SEVENSTER, HOOGLERAAR IN DE FACULTEIT DER GODGELEERDHEID, TEGEN DE BEDENKINGEN VAN DE FACULTEIT DER WIS- EN NATUURKUNDE TE VERDEDIGEN OP DONDERDAG 28 JUNI 1962 TE 15 UUR

DOOR

JÖRG REUSS

GEBOREN TE DÜSSELDORF (DLD.) IN 1929

'S-GRAVENHAGE
MARTINUS NIJHOFF
1962

Promotor: Prof. Dr. K. W. Taconis

CONTENTS

DESCRIPTION OF A 30 cm-H_2-BUBBLE CHAMBER

Summary

A detailed description of a 30 cm-H_2-bubble chamber is given. The simple cooling system, the expansion mechanism, which transfers the work under tension, the use of a tomback-expansion-bellows at liquid hydrogen temperatures, and the illumination system are unconventional.

Introduction. Starting in 1957 a H_2-bubble chamber was constructed and has been tested in several runs. It is a chamber with one horizontal window on top, a bellows for expansion at the bottom, a total volume of 19 l and a useful volume of 14 l.

The following represents an account of the work done and the experience gained during the years of construction and tests.

In chapter I general bubble chamber problems will be discussed in order to prepare the background, against which the special features of our chamber should be seen. The sections will deal with the general technique, the formation of bubbles, the guiding principles for the design, the accuracy of track location and the possibilities of a H_2-bubble chamber.

In chapter II a detailed description of all aspects of our chamber design will be given, with exception of the optical system. The general design, the mechanical construction, the cooling system and the expansion system will be treated.

The description of the optical system of our chamber will cover a relatively large part of this account. We shall discuss a special way to avoid disturbing reflections in a one-window-chamber, following a suggestion of Courant [14]). In the sections of chapter III the components of our optical system, bubble and source images, the illumination system and experiences with the flash lamp will be described.

CHAPTER I

GENERAL PROPERTIES AND POSSIBILITIES OF H_2-BUBBLE CHAMBERS.

§ 1. *On the general technique.* In 1952 D. A. Glaser [1]) proposed the bubble chamber as a new instrument of high energy physics. It was designed to meet the urgent demand for visible detection of fast particles produced in all the many accelerators which have recently come into being. The general idea of a bubble chamber is very simple. A superheated liquid starts to boil when disturbances are present. Fast moving charged particles can create such disturbances.

In § 2 we shall give a short discussion on the formation of bubble tracks. At this point it is sufficient to state that a chain of bubbles appears shortly after a charged particle has passed through the superheated liquid.

The chamber remains sensitive for bubble formation for a certain time only, because the superheated condition is unstable. The intention is to get the liquid back into the sensitive state at each synchrotron pulse. The whole working cycle runs as follows: The chamber liquid has a certain temperature T_0 and is pressurized slightly above its vapor pressure. To get it into the superheated condition the pressure in the liquid is suddenly decreased below the vapor pressure belonging to T_0. This is done either by enlarging the liquid volume in the case wherein no vapor phase exists in the then entirely closed chamber volume, or by expanding the vapor above the liquid in the case wherein the chamber is pressurized under a vapor phase. Now bubbles appear if "evaporation nuclei" are present.

The difficulty is that in the expanded state the liquid always starts boiling spontaneously. This causes the chamber pressure to rise until equilibrium between the liquid and the gas which boils off is reached. Then several minutes of recompression are required to re-establish the begin-conditions, because all of the evaporated gas has to be reliquefied. In order to reduce this time, a fast recompression is used before spontaneous boiling really starts. In the case of a hydrogen chamber, the total time during which the liquid is off pressure lies normally between 20 and 40 ms. Within this time the beam of particles must arrive, the bubbles have to grow to a visible size, and the flash has to work to get photographs of what has happened in the chamber. The repetition rate of expansion is normally ten per minute.

A bubble chamber may be used as a detector of particle tracks

when one is interested in reactions for which the chamber liquid itself is merely of secondary importance. In this case heavy liquids have the advantage of a high stopping power. Furthermore, molecules of high Z-numbers have a short mean free path for gamma rays. There exist, for example, xenon chambers with a mean free path of 6.4 cm for 100 MeV-gammas, which must be compared with a mean free path of 27 m in liquid hydrogen. In heavy liquids, however, multiple scattering effects are much more important than in liquid hydrogen. They impede accurate measurements of the curvature of tracks in a magnetic field, a quantity related to the particle momenta.

In general it can be said, that reactions producing gamma rays should be studied in heavy liquid chambers whereas in nearly all other cases liquid hydrogen chambers are preferable. A hydrogen chamber can also be filled with liquid deuterium. For the particles from an accelerator both hydrogen and deuterium contain target nuclei with a simple structure only, i.e. protons and deuterons respectively. In investigating the production of particles it is essential for later interpretation that the incoming particles react with such simple nuclei.

From the above it becomes clear that a bubble chamber is a measuring device very similar to the well-known Wilson chamber, with the advantage that the density of its liquid is much higher than the density of the gas which fills a cloud chamber. Thus the mean free path of a particle is considerably shortened. In a high pressure hydrogen cloud chamber working at 30 atm and room temperature, the mean free path for a hydrogen event is a factor 20 larger than in a hydrogen bubble chamber.

The general features of a hydrogen bubble chamber are summarized in the following table:

temperature	T_0	$= 27°\mathrm{K}$
pressure before expansion	p_0	$= 5.5$ atm abs.
pressure drop during expansion	Δp	$= 3$ atm
relative volume change during expansion	$\Delta V/V$	$= 0.01$
average size of a bubble	d	$= 200\ \mu$
time of bubble-growth	Δt	$= 1$ ms
number of bubbles/cm on a typical track	n	$= 15\ \mathrm{cm}^{-1}$
total time chamber is off pressure	$\Delta\tau$	$= 25$ ms
repetition rate	ν	$= 1\ \mathrm{s}^{-1}$
density of hydrogen	ρ	$= 0.059\ \mathrm{g.cm}^{-3}$
density of protons	N	$= 3.5 \times 10^{22}\ \mathrm{cm}^{-3}$

§ 2. *Bubble formation.* The formation of bubbles is still an open field in physics, as well for theoreticians as for experimentalists. Some new problems arise if one tries to understand the appearance of tracks in a bubble chamber. The fundamental question is, what does the passing charged particle do to the liquid so that a chain of bubbles is formed along its path. A further question is, how do the bubbles behave, once they are formed. Here one can apply the methods and formulas of the theory on the kinetics of boiling.

Glaser was the first to attack the fundamental question. He suggested that the electrostatic forces of ions were mainly responsible for the formation of bubble tracks in superheated liquids. Ions are created along the path of a charged particle. This point of view is similar to the normal treatment of droplet formation in a Wilson chamber.

In a superheated liquid a spherical bubble of a radius $r_c = 2\sigma \cdot (p_v - p_h)^{-1}$ is stable; p_v denotes the pressure inside the bubble and p_h the hydrostatic pressure in the liquid. r_c is called the critical radius. It is assumed that p_v equals the vapor pressure of the liquid. In a bubble with $r = r_c$ the overpressure $p_v - p_h$ inside the bubble is balanced by the surface tension σ. The surface tension causes a bubble to collapse if r is smaller than r_c, the overpressure forces a bubble to grow if r is larger.

The presence of a cluster of charged particles inside a bubble changes the situation. The repulsive force of charges of equal sign forbids a total collapse. Also with no overpressure inside a bubble there is a critical radius, at which the surface tension balances the electrostatic forces. Bubbles with $r = r_c$ are in real equilibrium, as all smaller ones tend to grow and all larger ones start to contract. With overpressure this critical radius increases, until at a certain value of $p_v - p_h$ all bubbles become unstable and begin to grow. This value of $p_v - p_h$ depends on the number of charges n inside the bubble. Glaser derives for it $(n \geqslant 2)$ $p_v - p_h = 5.62 \cdot \sigma^{4/3} \cdot E^{1/3} \cdot n^{-2/3}$. Here E is the dielectric constant of the liquid; the surface tension σ is measured in dynes/cm and the pressure p_v and p_h in atm.

With this expression the working conditions of most chamber liquids have been successfully predicted, assuming $n = 6$. The fundamental question, however, is only shifted thus far and not answered.

The existence of a cluster of charges with equal sign seems rather improbable in a liquid. The situation is very different from what one encounters in a Wilson chamber. There the occurrence of a single charge in a droplet produces a surface charge on the liquid-vapor interface as a consequence of the different polarization in the two phases. Normally the dielectric constant of the liquid is larger than that of the vapor. Therefore the surface charge has the same sign as the single charge inside the droplet. When the droplet is contracting, work must be done to bring the surface charge and the single charge nearer to each other. Therefore the same happens as in the case of a charge cluster inside a bubble. All droplets containing one single charge grow to macroscopic size if the difference between the chamber pressure and the vapor pressure exceeds a critical value.

In bubble chambers the difference between the dielectric constant of the liquid and the vapor works the wrong way if it is not negligible. Therefore one is forced to assume several charges of equal sign in a bubble if the electrostatic forces are responsible for the formation of bubbles.

In the handbook article on bubble chambers [1]) Glaser himself presents a series of arguments which make the electrostatic approach doubtful. Instead of repeating these here we only mention the total failure of the theory in explaining the behaviour of xenon. Pure liquid xenon could not be sensitized by expansion; when however, 2% ethylene was added, bubbles could be observed [1]).

In 1958 F. Seitz published an investigation concerning the possible connection between radiation damage in semi-conductors and bubble formation [2]). He considered knock-on-electrons as responsible for the occurrence of hot spikes in both cases. These electrons give off their kinetic energy over very short distances. In a superheated liquid, bubbles will grow explosively during 10^{-10}–10^{-11} s, before this heat accumulation disappears by conduction. With a final radius larger than the critical one they will have consumed the surplus of thermal energy inside the hot spike. In hydrogen under normal working conditions of bubble chambers the critical radius is about 10^{-7} cm. Once grown so far, the overpressure inside a bubble tends to increase its size further.

Seitz gives some estimates in his paper showing the physical possibility of this explanation. Although the way in which the results

are derived may be criticized, the underlying picture is generally accepted today.

The fact, that the behaviour of xenon finds a natural explanation favours this approach. Actually his experience with xenon led Glaser independently to the conception of rather the same mechanism of bubble formation. His guess that liquid xenon is a good scintillator is now confirmed experimentally. The xenon atoms which are excited by a fast ionizing particle will therefore loose their energy mainly by radiation. Addition of hydrocarbons or other quenching materials with many internal degrees of freedom brings about the possibility of converting the radiation energy into thermal energy. Thus also in liquid xenon a hot spike can be formed.

Experimentally little work has been done to clarify the situation. Feasibly strong electric fields would not influence the position of bubbles if they contained electrical charges. The flow resistance is too large and the time of growth too short for the bubbles to show displacements comparable to their diameters. Therefore, no indication can be expected from the application of electrical fields as to whether electrostatic forces play a role in bubble formation.

However, experiments have been performed with the aim of searching for a change in bubble density by action of an electrical field [3]). The magnitude of the used field of 15 kV/cm was supposed to be high enough to extract electrons out of a hot spike before a bubble assumes its critical size. Thereby recombination should be delayed. No measurable effect was found. It may be concluded, that either the heat of recombination is of minor influence on the formation of bubbles or that the recombination time is considerably shorter than 10^{-11} s, the time a bubble needs to grow to its critical size.

§ 3. *Guiding principles for the design of a hydrogen bubble chamber.* In this section we want to discuss some general points which determine the design of a bubble chamber by their relative importance.

The chamber volume must be illuminated and photographed to record what happens when a beam of particles is shot through. Use is made of the light scattering on the bubbles which mark the paths of the fast particles.

This scattering is mainly due to refraction effects. In principle

both, bright field and dark field illumination are possible for photographing the bubbles. In the first case the camera has to be placed in the path of the direct light, so that a decrease in light intensity can be seen. In the second case the camera receives the light which is scattered on a bubble, and the direct light is kept away. In practice the dark field illumination is generally preferred because of its better contrast.

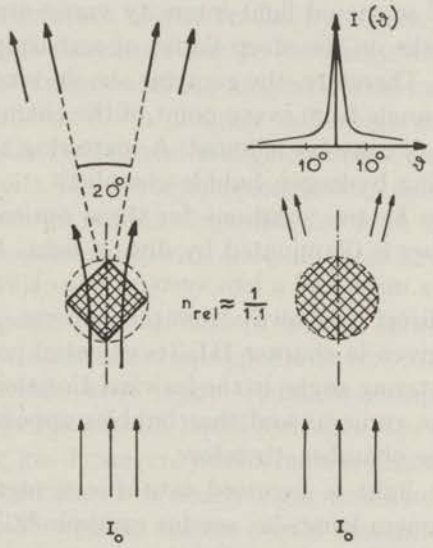

Fig. 1. Light scattering by bubbles. On the left a bubble is replaced by a double cone. n_{rel} is the refractive index between gaseous and liquid hydrogen at working conditions.

The distribution of the scattered light imposes some restrictions on a designer. By the following argument, one can get an idea of what the angular distribution looks like. Let us roughly approximate a bubble by a transparent double cone with its axis parallel to the incident light, as shown in fig. 1. A section through the cone axis should be a square with $\sqrt{2}$ times the bubble radius. Parallel light which falls on this double cone leaves it after being twice refracted at a fixed angle to the cone axis. This angle is a function of the relative refraction index between the double cone and its exterior. Assuming a value of 1.1 corresponding to the refractive index between a bubble and the bulk liquid hydrogen, we find the very small scattering angle of 10°. Instead of the fixed scattering angle,

a refined treatment gives an angular distribution, which is sharply peaked in the forward direction. About 12% of the scattered light is found within a cone of 6° halfangle from the forward direction, i.e. in 0.3% of the total angle 4π. For a more detailed discussion see chapter III and the literature given there.

This means that one has to provide for the possibility of photographing the bubbles at a very small angle from the direction of the direct light. The scattered light intensity varies strongly with this angle as one works on the steep flanks of a sharply peaked distribution function. Therefore, the cameras should receive light of the same scattering angle from every point of the chamber, otherwise a strong variation of contrast is found. A scattering angle of ca. 6° is typical of existing hydrogen bubble chambers.

There seem to be two solutions for these optical requirements:

1. The chamber is illuminated by diffuse light. By an ingenious arrangement of a mask and a lens system, Block *et al.*[4]) succeeded in keeping the direct light away from the cameras. A description of this method is given in chapter III. Its essential point is that light of nearly all scattering angles in the forward direction comes through the irises of the cameras and that bubbles appear equally bright in all parts of the chamber, therefore.

2. The direct light is focussed into the center of the circle, on which the camera lenses lie, see for example [5]). The bubbles are photographed therefore, in a slightly converging light beam. In practical cases the angle at which light is scattered into the cameras can thus be kept constant within ca. 10%. A certain non-uniformity of contrast is caused by this small variation. The high efficiency in the use of light makes the second method very attractive.

In both cases the chamber must have two windows on opposite sides or one window and a reflecting system. The light falls straight through the chamber or is reflected at the rear and leaves the chamber at the point of entry. Actually a window has to occupy the most of one chamber side so that the unilluminated regions are kept small.

Cold seals between a glass window and a metallic flange were unheard of before bubble chambers appeared. These seals have to remain good through several cool-down and warm-up periods. Nowadays, quite a number of satisfying solutions are in use, ranging from inflatable stainless steel tubes with adjustable inside pressure [6])

to simple metallic "O"-rings where the clamping flanges must possess some elasticity to account for different thermal expansions, see also § 7. To secure the tightness of the seal and to have a simple control of the remaining leak rate, double seals are normally applied with a pump-out line in between.

There is another particular connected with the requirements of illumination and photography. As the particle momenta are displayed in the curvature of the tracks by action of a magnetic field, and as this curvature has to be easily detectable on the photographs, the direction of the magnetic field must be perpendicular to the windows. For a designer this means that the chamber walls parallel to the field direction should be most closely surrounded by the magnet coils. The use of pole pieces interferes with the necessity that the windows remain accessible for both illumination and photography. Constructions with one pole piece have been realized, see for example [6]).

From a cryogenic point of view a bubble chamber is a rather unsatisfying instrument if not equipped with its own refrigeration system. The whole heat input would be compensated for by evaporating of the coolant, i.e. liquid hydrogen. The cooling capacity of the returning gas however, would remain unused. The amount of heat the gas can absorb is nearly eight times its heat of vaporization. A reversible cooling system would consume 6190 J to cool 1 g of H_2 at the constant pressure of 1 atm from 300°K down to 20.4°K and another 6220 J to liquefy it. Consequently if the evaporating gas is simply blown off the same refrigeration can be effected at the cost of twice the power which would be consumed in the case where the cooling capacity of the evaporating gas is utilized. In all practical cases this difference in power consumption is considerably greater due to the irreversible character of the various processes, which take place in a refrigerator or liquefier.

Furthermore, it is advantageous to work with a closed refrigeration system if long runs are performed whereby 20–30°K are maintained inside the chamber during several weeks or longer. In a closed system, heat exchangers and expansion devices can easily be kept free of moisture for these long periods.

On the other hand, to build a refrigeration plant which could absorb heat at the temperature of liquid hydrogen takes so much time that the final decision depends on the hydrogen consumption

and the liquefying facilities already existing. One should accept a less efficient external system, if a large enough one is already in being, or if one should have to be built for other purposes.

The bubble chamber must be surrounded by radiation shields to decrease the static heat loss. Normally hydrogen chambers with a volume of 10 to 20 l have a static heat loss corresponding to an evaporation of 1 to 3 l of liquid hydrogen per hour.

As for the dynamic heat loss, we have to discuss liquid expansion and gas expansion separately. What happens in the case of liquid expansion is demonstrated in fig. 2. During expansion a change of the chamber volume of about 1% causes the pressure to drop from 5.5 atm to 3 atm. This pressure drop is due to the elastic expansion of the bulk liquid, as no vapor phase exists in the entirely closed

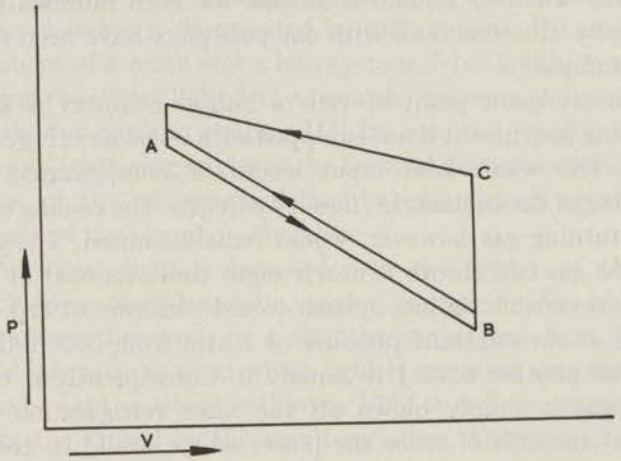

Fig. 2. Schematic P–V-cycle for liquid expansion, (A–B–A) fast recompression, (A–B–C–A) slow recompression.

chamber volume. The expanded chamber is at the point B of the diagram and has to return to point A. There are two limiting possibilities: either so fast a recompression is used that the returning line in the diagram almost coincides with the line from A to B, or recompression begins so slowly that the chamber is fully pressurized by spontaneous boiling, beforehand. Then the returning line goes via C. In both cases the curves enclose an area equal to the mechanical work which is delivered to the chamber during one expansion cycle. In the worst case (A–B–C–A) this area corresponds to the

heat of vaporization of ca. 0.05 l of hydrogen/h per liter of chamber, assuming one expansion every 5 seconds. In all practical cases the time between expansion and compression is made as short as possible, of course, so that the heat loss per expansion cycle is kept at a minimum.

A piston system is installed on top of some chambers; it is in contact with the chamber liquid and provides for the necessary volume change. Others are expanded by means of a bellows. Both bellows and piston are driven from the outside.

In the case of piston expansion the liquid level stands above the piston. Therefore, during an expansion no gas enters the chamber through the small leak along the cylinder wall. One drawback is that the liquid on top of a piston splashes during the expansion stroke causing heat losses which exceed the theoretical value given above. From the data of existing chambers, one can derive the average value of dynamic heat loss corresponding to the heat of vaporization of 0.1 l of hydrogen/h per liter of chamber, assuming one expansion every 5 seconds [7]). The use of a piston limits the freedom of design, as the piston must always be mounted on top of the chamber because of the unavoidable leakage along the cylinder wall.

The bellows system does not show these disadvantages. There is no reason why the theoretical value of dynamic heat loss should not be found in practice, or why the bellows should not be mounted wherever desirable. But here the finite lifetime of a bellows is the problematic point. So far bellows have not been used in large chambers. In smaller chambers mainly stainless steel bellows are applied, both of the welded and of the unwelded type. Volume changes of a few hundred cm^3 are achieved.

Liquid expansion is superior to gas expansion, if one wants to minimize the dynamic heat loss and tries to work with the shortest possible expansion-recompression cycle. On the other hand, all essential parts like the bellows or the cylinder and the piston are mounted in a position where repairing is impossible without warming up the whole chamber and thus interrupting a run for a rather long time.

The great advantage of gas expansion is its simplicity and the possibility to mount all essential parts where they can easily be replaced during a run. In gas expansion, the cold vapor above the liquid is expanded into a buffer volume at room temperature, then

TABLE I

Data of existing or designed bubble chambers						
Place	Dimensions	Year of Completion	Useful Volume l	Total Volume l	Window	Expansion System
Saclay	35 cm ⌀	1960			2 vertical	piston
Saclay	50 cm ⌀	1960			2 vertical	piston
Saclay	80 × 30 × 30 cm³	1961			2 vertical	piston
Liverpool	25 cm ⌀	1960	3		2 vertical	bellows
Birmingham	9″ ⌀ ; 4″ deep	1960	3,4	5,5	2 horizontal	bellows
Imperial Coll. London	40 cm ⌀ 15 cm deep	1960			2 vertical	vapor exp.
British National Project	150 × 50 × 45 cm³	1962			2 vertical	vapor exp.
Bologna	18 cm ⌀ 12 cm deep	1959	2,5	3	2 vertical	bellows
Leiden	30 cm ⌀ 20 cm deep	1961	14	19	1 horizontal	bellows
Cern	32 cm ⌀ 15 cm deep	1960	9,5	13,4	2 vertical	piston
Cern	200 × 60 × 50 cm³	1963		1000	2 vertical	
Berkeley	10″ ⌀	1956	8		2 horizontal	vapor exp.
Berkeley	15″ ⌀	1958	20	40	1 horizontal	vapor exp.
Berkeley	72″ × 20″ × 15″	1959	300	500	1 horizontal	vapor exp.
Berkeley	25″ ⌀ ; 15″ deep	1962			2 horizontal	piston
Columbia	12″ ⌀	1957			2 vertical	bellows
Brookhaven	14″ ⌀ ; 8″ deep	1959			2 vertical	piston
Brookhaven	20″ × 9″ × 10″	1959	28	60	2 vertical	piston
Brookhaven	80″ × 25″ × 28″	1961	900	1700	1 vertical	piston
Chicago	23 cm ⌀ ; 15 cm deep	1960	6		2 vertical	bellows
MIT	40″ ⌀	1962	500	600	1 vertical	piston
Wisconsin	30″ ⌀ ; 15″ deep	1962			2 vertical	piston

TABLE I (*continued*)

Data of existing or designed bubble chambers				
Place	Number of Cameras	Film Size mm	Magnetic Field kG	Particular Properties
Saclay	3	35	17	
Saclay	3	35	17	
Saclay	3	35	19	
Liverpool	2	35	8	stainless steel bellows of 8″ free length
Birmingham			22	pulsed magn. field. Coils aircooled. stainless steel bellows 4″ ⌀ ; 5″ long
Imperial Coll. London	3		18	
British National Project	3	35	12	illumination system which allows photography at 2° scattering angle
Bologna	3	35	15	welded stainless steel bellows
Leiden	3	35	(12)	tomback bellows 210 cm ⌀ ; simple mirror
Cern	3	35	15	
Cern		50	15	closed H_2-refrigeration system utilizing turbines for expansion
Berkeley	2	35	12	diffuse illumination with venetian blind system; one pole piece
Berkeley	4	35	10	retrodirective reflecting system (coat hanger); one pole piece
Berkeley	3	50	18	coat hanger; tilted window
Berkeley	3			the upper window serves as a piston
Columbia	3	35	13,4	max. repetition rate 2/s; welded stainless steel bellows
Brookhaven	3	35	17,5	
Brookhaven	4	35	17	magnet coils inside vacuum tank; chamber body made of an Al-forging
Brookhaven	4	35	17	simple mirror; one pole piece
Chicago	3	35	20	chamber for stopping particles
MIT	4	35	20	closed He-refrigeration system
Wisconsin		70	30	3–4 megawatts magnet power

recompressed, cooled down to liquid nitrogen temperature and finally used to pressurize the liquid volume again. During the pressure drop the liquid rises somewhat in the expansion line, starts to evaporate until a cold surface layer is formed, and is pressed back by the recompression. Here the dynamic heat loss is determined by the amount of gas which evaporates from the liquid at 25°K during the expansion and has to be reliquefied when it comes back during recompression at a temperature of about 80°K. The problem is how to avoid drastic splashing in the expansion line. Because of expansion speed, and in order to keep the level differences of the liquid small, this line leads through a very wide pipe which makes it nearly impossible to avoid sensible heat losses by splashing. The average loss derived from existing chamber data is 0.5 l of hydrogen/h per liter of chamber, assuming one expansion every 5 seconds [7]).

At the end of this section we present a table of hydrogen chambers already working or under construction in Europe and the U.S.A. Small chambers with diameters less than 10 cm are omitted.

The *useful volume* is the illuminated volume, where tracks can be photographed. The *total volume* gives the liters of liquid hydrogen in the chamber not counting reservoirs. Under *windows* their number and position is given. The information under *expansion system, magnetic field, number of cameras* and *film size* needs no further comment.

The construction of the Leiden bubble chamber was started early in 1957. At that time the technique of hydrogen chambers showed two lines of development. 1) The Berkeley group under Prof. L. Alvarez favoured gas expansion and horizontal windows. Several chambers of increasing size had been built or designed. 2) The group under Prof. J. Steinberger at Columbia University preferred liquid expansion with a bellows system and vertical windows. Later on Shutt and Adair of Brookhaven perfected this chamber type introducing a piston system instead of the bellows.

Most ideas for more recent chamber designs are derived from these two "schools". Except for the expansion system our chamber resembles the Berkeley 15″-chamber. Both of them were designed independently at about the same time. For expansion a bellows is placed at the bottom of our chamber.

§ 4. *Accuracy of track location.* In the following the total resolution in space which can be achieved with a hydrogen bubble chamber will be discussed. Further, how far secondary effects like convective movements of the chamber liquid influence the accuracy of track location will be investigated.

Each bubble needs some time to grow from its critical dimension to a visible size. As mentioned in § 2 the critical radius is about 10^{-7} cm. The term visible size cannot be well defined, as it depends on the light intensity with which the chamber is illuminated. The time of bubble-growth is kept so small that the actual size of a bubble at the moment of photography does not influence the space resolution, i.e. the dimensions of the image of a bubble on the film are entirely determined by the emulsion properties and diffraction effects. A further decrease of the bubble-growth time would merely produce worse contrast, because less light per bubble is scattered.

In normal bubble chamber work, the resolving power attained with a depth of focus of about 25 cm is 50 bubbles/cm. In hydrogen the bubbles are allowed to grow for 1 ms or less. The real bubble diameter is kept well below 200 μ.

Assuming that the track center can be located within 1/10 of the width, one finds a minimum uncertainty of position equal to $2 \cdot 10^{-3}$ cm. Some slight improvement may be brought about by the use of an annular diaphragm, as the British Bubble Chamber Team proposes [8]). The depth of focus increases if the center region of an iris is covered by a disc and its diameter correspondingly enlarged so that the same amount of light is transmitted. Therefore it should be possible to work with a smaller effective stop using an annular diaphragm and yet achieve the same depth of focus. Diffraction effects should become small enough so that the resolution would be limited mainly by the properties of the emulsion.

During the time the bubbles grow to visible size, tracks may be distorted due to the convective movements in the chamber liquid and to the liquid flow started by the expansions. As long as the distortions are systematic it is possible to correct for them. Here we only are interested in irregular distortions which may reduce the accuracy of locating the actual track.

There will be no convection in the chamber if the thermal insulation is ideal. However, with a heat input due to radiation, expansion etc. convection is essential for maintaining a uniform

temperature in the liquid, because liquid hydrogen is such a poor conductor. The influence on the track quality remains small if the time for bubble-growth is small.

After an expansion the forced movement of the liquid does not cease immediately, as the decay time of a vortex is of the order of 10 minutes [9]). To avoid difficulties due to this, the chamber has to be expanded as homogeneously as possible, and again the time of bubble-growth must be small.

Few new restrictions on the track quality will arise, if this time is about 1 ms and the chamber has been carefully designed with respect to these effects. Measurements by the CERN-group show that under optimal conditions the unsystematic deviations from the systematically smoothed tracks are smaller than $3 \cdot 10^{-3}$ cm [10]). The setting error of the measuring device IEP in this investigation was $(2.4–2.7) \cdot 10^{-3}$ cm. Therefore this result means that the locating of particle tracks is not seriously, if at all, affected by distortions.

The above considerations show that it should be possible to construct a hydrogen bubble chamber which allows a track definition within $2 \cdot 10^{-3}$ cm.

§ 5. *Possibilities of a hydrogen bubble chamber.* In this section we will examine what information can be extracted from bubble chamber photographs. The first part deals with directly observable charged particles, the determination of their momenta, their ranges etc. In the second part the identification of uncharged particles will be touched upon.

Charged particles mark their way through the liquid by a chain of bubbles. Momenta can be determined by bending the tracks in a magnetic field and measuring their curvature. The relation between momentum and curvature is $p \cos \delta = nKrB$, where $K = 0.3$ cm^{-1} kG^{-1} MeV/c, r = radius of curvature in cm measured on the parallel orthogonal projection of a track into a plane perpendicular to B, n = charge of the passing particle in units of the electron charge, B = magnetic field in kG, p = momentum in MeV/c and δ = angle between the track and a plane perpendicular to B. If multiple scattering is neglected a maximum momentum of 15 GeV/c can be detected on a track of a length $L = 10$ cm in a field of 12 kG, corresponding to a radius of curvature $r_l = 40$ m. For higher momenta the curvature disappears in the minimum track

width which has been discussed in the preceeding section. The maximum detectable momentum is proportional to L^2.

Multiple scattering, however, impairs this result at least for particles with small energies. For protons and pions the apparent radius of curvature r_{sc} due to multiple scattering in liquid hydrogen is given as a function of energy in table II. A track length of 10 cm is assumed. As $r_{sc} \sim L^{\frac{1}{2}}$ one easily finds r_{sc} for other values of L.

TABLE II

Track properties of protons and pions

Ranges are given for liquid hydrogen. r_m is the radius of curvature as consequence of a magnetic field. Multiple scattering causes a curvature of tracks with the average radius $\pm r_{sc}$

kinetic energy MeV	range proton cm	$B \cdot r_m$ proton kG·m	r_{sc} proton m	range pion cm	$B \cdot r_m$ pion kG·m	r_{sc} pion m
10	1	4.60	1.66	4	1.80	1.79
50	17	10.50	7.82	75	4.30	7.25
100	65	14.80	14.80	200	6.50	13.10
500	850	36.30	60.20	1700	20.80	36.70
1000	3000	56.50	104.00	3500	37.70	81.30
5000		195.00	381.00		172.20	340.00

The radius r_{sc} must be compared with the magnetic radius r_m which follows from the values Br_m in table II. Because r_{sc} indicates a curvature in an arbitrary direction due to a large number of uncorrelated small angle scattering processes, the magnetic radius r_m can only be measured if it is smaller than r_{sc}. The relative error in the momentum measurements can be estimated as follows: $\Delta p/p = r_m/r_0$, with $r_0^{-2} = r_l^{-2} + r_{sc}^{-2}$.

To identify a particle it is necessary to know a second independent parameter besides the particle momentum. Ranges are normally too large to be measured as an inspection of table II shows. There is the possibility of counting the number of bubbles per unit track length or, rather, measuring the mean gap length between them. These quantities are related to the number of δ-rays per unit track length. Before advantage can be taken of these measurements, empirical relations with energy and restmass have to be established [11]). For relativistic particles no variation of the mean gap length with momentum has been found in liquid hydrogen. Therefore this sort of measurement yields information only in the low energy range.

Uncharged particles do not leave a track in a bubble chamber. Nevertheless track chambers are indispensable when unstable uncharged particles are studied, as for example the K^0, Λ^0 and Σ^0. Production and decay processes of these particles involve at least two outgoing reaction products, whose kinematics must be known simultaneously. For example, the following reaction is possible: $\pi^- + p \rightarrow \Lambda^0 + K^0$. Both secondaries are invisible and have to be identified by their decay products. Let us assume the following decay modes $\Lambda^0 \rightarrow p + \pi^-$ and $K^0 \rightarrow \pi^- + \pi^+$. The analysis of such an event starts from the end. The momenta of the invisible particles are determined from the momenta of their charged decay products. Then the mass of the uncharged particles is determined by checking energy conservation. For this the energy of the incoming particle must be known. One hopes that all but one possibility can be rejected, so that finally a clear picture of the event arises.

Complicated reactions like this one cannot be studied in counter experiments. The only way to study a reasonable number of events of this kind is by the use of a track chamber in a high energy beam from an accelerator.

Table III contains all known particles with exception of the antiproton, antineutron and antilambda. It is meant to give a clue about the needed dimensions of a track chamber, if decay processes of one of the unstable particles should be observed. The *decay length* L_0 for $\beta^2 = (v/c)^2 = \frac{1}{2}$ is given.

In table III the particles are divided into four groups: 1. stable particles; 2. long lived unstable ones whose decay can only be observed in bubble chambers when they are captured or come to rest there; 3. the particles with a medium life time, which decay after a reasonable track length unless their total energy exceeds their rest energy by many orders of magnitude; 4. the short lived particles which decay at their "point of origin" within the accuracy of a bubble chamber, at all feasible energies at least.

We conclude this section with two remarks mainly concerning our 30 cm bubble chamber:

A secondary, produced in the center region of our chamber, has a track length of about 10 cm before it leaves the chamber. A mean free path of 10 cm corresponds to a cross-section of $3 \cdot 10^{-24}$ cm^2 in liquid hydrogen. A cross-section of this large size never occurs in

high energetic collisions with protons, and therefore an interaction of a secondary cannot be observed.

TABLE III

Characteristic figures for the decay of elementary particles
L_0 must be multiplied by the dimensionless quantity pc/m_0c^2 to obtain the actual decay-length L for a particle of rest mass m_0 and momentum p

type of particle	decay products of a possible mode	reduced decay-length L_0 cm	kinetic energy when $L = 10$ cm MeV	approx. rest energy MeV
stable particles				
γ	–	∞	–	0
$\nu, \bar{\nu}$	–	∞	–	0
e^+, e^-	–	∞	–	0.51
p	–	∞	–	938
particles with long lifetime				
μ^+, μ^-	$e + 2\nu$	6.6×10^4	0	106
π^+, π^-	$\mu + \nu$	7.7×10^2	0	140
θ_2^0	3π	1.8×10^3	0	498
K^+, K^-	3π, 2π, etc.	3.7×10^2	0	494
n	$p + e + \nu$	3.0×10^{13}	0	939
particles with medium lifetime				
θ_1^0	2π	3.0	1210	498
Λ^0	$N + \pi$	7.5	740	1115
Σ^+	$N + \pi$	2.4	4150	1189
Σ^-	$N + \pi$	4.8	1550	1196
Ξ^-	$\Lambda^0 + \pi$	4.0	2250	1318
particles with short lifetime				
π^0	2γ	5.7×10^{-6}	2.4×10^8	135
Σ^0	$\Lambda^0 + \gamma$	< 0.3	$> 4 \times 10^3$	1191

Assuming a cross-section of 10^{-28} cm^2 there will be one event on 3 km track. In our chamber we will work with ca. 10 incident particles, having a usable track of 2 m/photo. Therefore a cross-section of 10^{-28} cm^2 will mean one event per $1.5 \cdot 10^3$ photos. The chamber has to work 2h to take these $1.5 \cdot 10^3$ photos. Six man-days are necessary merely to scan them. If 100 events are wanted it takes considerably more than two man-years for their complete evaluation. Consequently a cross-section of 10^{-28} cm^2 can be regarded as the minimum for our bubble chamber without pre-selection of events.

CHAPTER II

CHAMBER CONSTRUCTION AND PERFORMANCE.

§ 6. *General design.* The general design of the Leiden bubble chamber is founded on the following arguments.

1. We wanted to build a helpful tool for high energy physics, intending to do experiments at the 1 GeV proton accelerator in Delft. We decided to construct a chamber with a diameter of 30 cm and a depth of 20 cm. When we started the construction in 1957, a 30 cm chamber was quite a big one. Its usable volume of 14 l was – and still is – thought to be sufficient for most of the experiments that can be done at a 1 GeV accelerator.

2. As we wished to reduce the danger of window failure we have been led to a construction with one window. This implies the use of a mirror system. The flash lamp then doubly illuminates the chamber: once directly and once after the light is reflected by the mirror. A bubble scatters the light in forward direction, and is therefore seen by a camera once directly and once in the mirror. Consequently two images of each track appear on the film. The second image is seen behind the mirror. On the film it appears unsharp as it is normally out of focus for the cameras. In our experience it has been possible to set the focus of the cameras so that the second track image disappeared in the background, unless the corresponding tracks were formed in the vicinity of the mirror.

3. The most controversial question was whether to put the window horizontal or vertical. Both propositions have a number of advantages and disadvantages. Again our main argument was to achieve a maximum of safety. A horizontal window was chosen as it allows a construction where the chamber hangs in a sort of cryostat. This cryostat or vacuum tank can be used as a hydrogen reservoir or can be kept at a rough vacuum; in both cases it works like a cold buffer volume into which the pressurized hydrogen can expand in case of window failure. If the vacuum tank is built to withstand the pressure shock, such a system is rather safe.

We keep the vacuum tank, which of course is high vacuum insulated from outside, at a pressure of 10^{-1}–10^{-2} mm Hg. This gives another advantage: the cold seal between the window and the metallic chamber body need not be high vacuum tight, as the thermal insulation does not depend on it. What leaks out of the

chamber into the cryostat space must be replaced by condensation, this being the limiting factor for the tolerable leakage rate in our case.

Furthermore the horizontal window construction makes it easier to get a beam through the chamber, whatever its energy. Trouble namely can be caused by the magnetic stray field outside the chamber which bends the beam out of its original direction. As long as this happens in a horizontal plane by action of a vertical field, it only influences the position of the chamber. But if the beam is bent out of the horizontal plane by action of a horizontal field a compensating magnet has to be used. Otherwise the mean beam direction inside the chamber will be inclined with respect to the horizontal plane, demanding the chamber to be tilted. Such an unpleasant horizontal stray field happens to be connected with the use of vertical windows.

One must be very careful to avoid a temperature gradient in the hydrogen volume, if one has a chamber with a horizontal window on top. Most of the heat leakages come from above. The chamber is open to thermal radiation from the warm top flanges there (see fig. 3), and the suspension and pipe connections conduct heat to the upper part of the chamber. Futhermore all bubbles rise a little bit during the expansion time, giving back the heat of vaporization to the chamber liquid at a place somewhat higher than where originally taken from. Therefore it is possible that the temperature increases in an upward direction. A temperature gradient occurs easily, especially just below the horizontal window where no convection can take place. If the top layer is only slightly warmer there will arise no difficulty unless spontaneous boiling disturbs the view of the cameras. However, it is still true that there will be a higher sensitivity for bubble formation. Also, the speed of bubble growth will be larger there, but it only means that tracks in this top layer must not be used for bubble counting. In chambers with vertical windows a tendency to build a warm top layer exists, too, but here this top layer belongs to the unilluminated and unused volume. Normally the expansion system is mounted on top of this type of chamber. Its moving parts cause an irregular flow there, which helps to prevent a temperature gradient.

In our experience, perhaps, the most serious argument against a horizontal window is that dirt tends to settle on the optical components. Inside the chamber frozen out impurities fall on the mirror

and disturb the dark background, and outside abrasion products of the mechanical connections to the expansion system partly terminate on the window.

4. Liquid expansion was chosen because of the possible high repetition rate. Furthermore it should give fewer unsystematic track distortions. The simplest way to fit liquid expansion to our general design idea was to make the bottom of the chamber movable by means of a bellows. The chamber can expand by its own pressure and can be recompressed moving back the chamber bottom with help of a mechanical system.

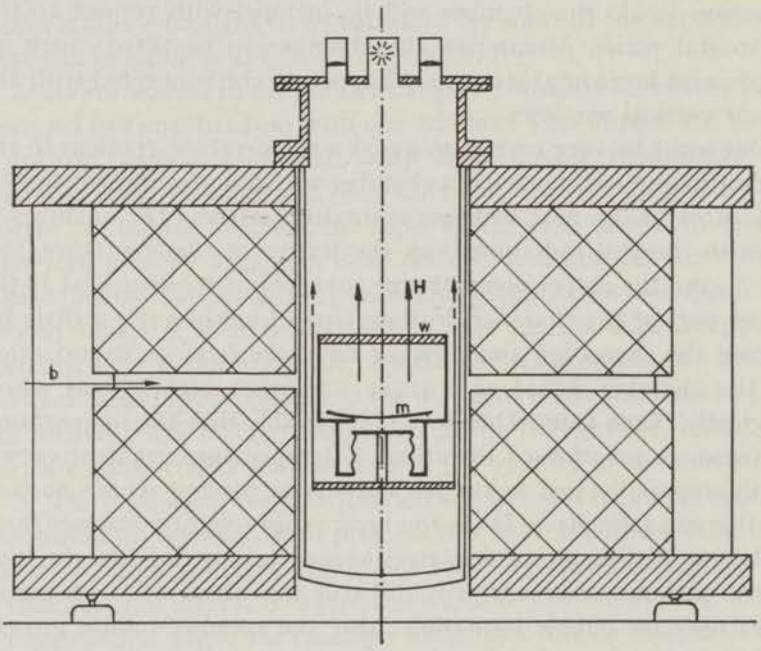

Fig. 3. The chamber construction. *b* means beam direction, *m* mirror, *w* window and *H* magnetic field. The true height of the magnet is ca. 1 m.

5. The magnetic field which serves for the detection of particle momenta is created by two coils around the vacuum tank. The chamber is accessible to the beam through a small space between the coils. Using an iron yoke to concentrate the back flux, the forces between the coils are compensated for a great deal and the central field is increased. Operators are protected by the magnetic structure. We plan to work with a total field of 12 kG. The power consumption

of the magnet is anticipated to be 450 kW at this field strength.

These five arguments give account of the general how's and why's in our construction. In fig. 3 the actual design is summarized.

Here we should like to comment on one point, in which our chamber probably differs from all the others, which are existing. The Leiden chamber had to be built inside the normal laboratory routine and it should possess such a simplicity that it could be run by one physicist with some technical help. At the end of the construction we can state that the chamber has been built in four years at the cost of 45,000.— Dutch Guilders excluding the cost of the magnet and salaries, using four years of a full time physicist, three years of part time students, four years of a young technician. Large profit was taken, of course, from the stock of experience in all sorts of techniques which is on hand in the Kamerlingh Onnes Laboratory.

§ 7. *Mechanical construction.* The body of our chamber is made of stainless steel type 304. Some parts are machined from forged flanges and are not as unmagnetic as the rest. All joints are argon arc welded.

The major parts of the construction were built in the workshop of the "Veluwsche Machinefabriek" in Epe (Netherlands), in close collaboration with Mr. E. S. Prins of our institute.

The chamber consists of five stainless steel cylinders and flanges as shown in fig. 4. They are clamped together with "O"-ring seals in between them. We have chosen this design to ensure a cheap construction and an easy operation when the mirror, the bellows or the window must be replaced. The cylinder enclosing the illuminated volume can be exchanged. We shall have built some spare cylinders with different beam windows to meet various experimental requirements.

The glass is mounted excentrically on the upper flange. In this way one has enough space on one side of the top flange to connect all necessary tubes like the filling line, the evaporation line etc. to the chamber.

The "O"-rings are made of drawn copper wire with a rectangular cross-section. The annular sealing surfaces have a width of 2 mm and are covered with a thin indium film. The variation in height, especially where the two ends of the copper profile are silver soldered to form a ring, amounts to 0.10 mm. We could leave these

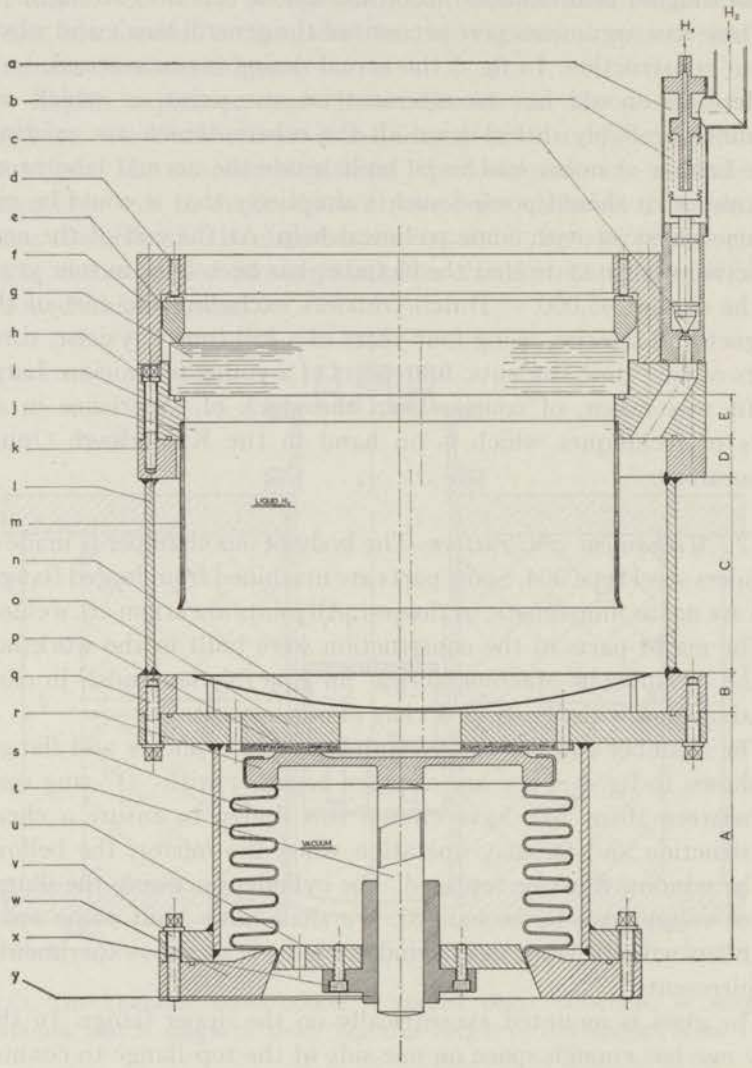

Fig. 4. The chamber body. (Scale 1 : 5).

One H_2-line is visible, which enters the chamber from above via a bellows valve and ends in the chamber behind the copper cylinder.

A = 162 mm
B = 25 mm
C = 130 mm
D = 25 mm
E = 27 mm

a one of the two bellows valves, which are operated by helium gas; under working conditions these valves allow one to disconnect the filling line and the evaporation line from the chamber.

b two-ply stainless steel bellows, 20 convolutions and 42 mm length.

c metallic sealing: brass cone against stainless steel; the approximate leakage is 10 cm^3/s under working conditions at 1 atm pressure head across the valve.

d 36 Allen screws M6 which provide the needed sealing force for the glass to metal seal *h* between *g* and *i*.

e a massive copper ring distributes the sealing force homogeneously over *h*.

f "L"-shaped flange works like an elastic strip under a bending moment. It is fixed on *i* by 24 screws M8 located between the 24 screws indicated by *k*.

g window of tempered BK 7 glass, 300 mm in diameter and 35 mm thick.

h "O"-ring of annealed copper which is covered by a thin indium film.

i excentric flange where all connections to the chamber enter; the smallest inner diameter is 280 mm.

j indicates the position of 4 M3 screws, which fix *m* on *i*.

k 24 M8 screws, which provide the needed sealing force for the metal to metal seal between *i* and *l*; the seal consists of an "O"-ring similar to *h*.

l cylinder with flanges which encloses the illuminated chamber volume; 320 mm and 336 mm are the smallest and the largest inner diameters, 370 the largest outer diameter, 5 mm the wall thickness.

m copper cylinder inside the chamber which serves to minimize temperature differences and track distortions; its wall thickness is 1 mm.

n chromium plated brass mirror of 300 mm diameter with a radius of curvature of 1209 mm.

o flange at the bottom of the illuminated volume; several holes provide the connection to the expansion bellows *s*.

p leather ring, which serves as shock absorber; the air driven piston on the other side of the expansion system outside the vaccuum tank is stopped by a rubber shock absorber, before *r* hits *p*.

q 24 M8 screws, which provide the needed sealing force for the sealing between *o* and *l*; the seal consists of an "O"-ring similar to *h*.

r movable chamber bottom, drawn in a position when the chamber is pressurized; it is made of brass and soft soldered to the bellows *s*.

s tomback bellows (80% Cu, 20% Zn), 2 mm wall thickness, 6 convolutions and 295 cm^2 average surface.

t stainless steel plunger, which transmits the force, needed for the re-compression, to the movable chamber bottom *r*; its wall thickness is 1.5 mm.

u stainless steel flange, which is soft soldered to *s* and *w*; simultaneously it is kept in position by stainless steel strips fixed on *w*. These strips are not drawn; the small hole on the left is the only connection between the space inside the bellows *s* and the vacuum tank.

v 24 M8 screws, which provide the needed sealing force for the "O"-ring seal between *o* and *w*; the "O"-ring is similar to *h*.

w stainless steel flange, which closes the chamber from below; its outer diameter is 315 mm.

x 6 M6 screws, which fix *y* on *u*.

y brass cylinder guides the plunger *t*.

sealings untouched for several runs without finding untolerable leaks developing.

The glass window is sealed to the chamber body in a very similar way. As can be seen in fig. 4 the glass is held down to its sealing by a massive ring of copper. The contact surface between this ring and the glass has an annular shape of about 2 mm width. Its position is just opposite of the sealing surface on the other side of the glass. The copper ring serves to equilibrize the sealing force over the whole contact surface and to partially compensate for the difference in thermal contraction between glass and stainless steel. The sealing force is created and transmitted to the copper ring by means of 36 Allen screws M6, placed at a distance from each other of about 25 mm.

The "L"-shaped stainless steel flange, which surrounds the copper ring, acts as an elastic strip under a bending moment. It helps to avoid a fatal increase of the sealing force due to the different thermal contraction of the glass-, stainless steel- and copper parts, when the chamber is cooled down.

During our first runs we worked with windows of untempered optical glass. Although we changed over to tempered glass it is perhaps worthwhile to describe this early experience.

Peak values of stress occur where the metallic "O"-ring touches the glass. These may not surpass the breaking stress of glass which is 450 kg/cm^2 (untempered) and 2,000 kg/cm^2 (tempered) at room temperature [12]). The breaking stress times the sealing surface gives the maximum force f with which the glass may be clamped to the chamber body. Our window has a diameter of 30 cm and the diameter of the sealing surface is 29 cm. Therefore we find the limit values for f: $f = 41\ d\ \mathrm{t}$ (untempered) and $f = 182\ d\ \mathrm{t}$ (tempered). d is the width of the annular sealing surface in cm.

It is necessary that f exceeds the force with which the pressurized hydrogen in the chamber acts in the opposite direction on the window, i.e. ca. 4t. Under working conditions we have 6 atm abs. inside the chamber and vacuum outside. Consequently d must be larger than 0.1 cm in case untempered glass is used.

We had chosen, therefore, a copper "O"-ring with a square cross-section, $d = 0.2$ cm. The manufacturing tolerances of this glass to metal seal had to be very stringent. A variation in height of 0.1 mm was fatal for untempered glass.

With a carefully built "O"-ring of square cross-section we cooled down the chamber to liquid hydrogen temperature and everything worked fine. The untempered glass seemed to stand the test. But when we inspected the window thoroughly a week later we discovered a lot of barely visible radial cracks at every place where the "O"-ring had touched the glass.

With tempered glass a square cross-section of the "O"-ring is unnecessary as our above estimate suggests and experience shows. d must be larger than 0.02 cm. The manufacturing tolerances of an "O"-ring with a circular cross-section are less stringent. In its position under pressure it is deformed into an oval shape, so that small differences of height are smoothed out. This deformation is possible because the yield strength of annealed copper (800 kg/cm^2) is smaller than the breaking strength of tempered glass (2,000 kg/cm^2) at room temperature. The "O"-ring surface is covered with a thin indium film to improve the sealing.

The total leakage between the chamber and the outside cryostat normally does not exceed 0.5 l NTP per hour at a pressure difference of 1 atm. Four "O"-ring seals with a diameter of about 30 cm each and several small ones contribute to this rate. During the cool-down period thermal stresses deform the sealing flanges so that 100 l NTP/h may escape for a time.

Inside the chamber a 1 mm thick copper cylinder is mounted, which surrounds the illuminated volume. It prevents a temperature gradient in the liquid volume and helps to get a uniform flow pattern during the expansion. Between this copper cylinder and the chamber walls a cooling spiral and some thermometers are located. Also the filling line and the evaporation line end there.

The whole chamber is suspended by three stainless steel tubes from the top flange of the vacuum tank. All pipes (filling-, evaporation- and condensing-line, inlet and outlet of the cooling spirals, gas- and vapor pressure- thermometer) and four thermocouples are connected to the chamber from above as in normal cryostat technique.

The vacuum tank is built from two thin-walled stainless steel cylinders with curved bottoms leaving space for a high vacuum insulation in between. It has heavy iron flanges on top, from which the chamber is suspended and which support the optical components.

The magnet is planned to surround the vacuum tank which will hang in the top flange of the iron yoke, as shown in fig. 3.

§ 8. *Cooling system.* The cooling system of our chamber is shown in fig. 5. 3 m of a spiraled $\frac{1}{4}''$ copper tube run through the liquid in the upper part of the chamber, figuring as an evaporator. Parallel to it and for the same purpose 1 m of $\frac{3}{4}''$ copper tube is mounted in direct contact with the upper flange. This line has its own return tube so that the flow through it can be regulated separately.

In these tubes liquid hydrogen is evaporated at a temperature of 20°K. It is fed into the evaporators directly from a hydrogen storage vessel, in which the pressure is kept at 1.2 atm abs. The returning gas is blown into atmosphere or sent back into a gasometer. It passes through a valve at room temperature by which the amount of evaporating refrigerant is regulated by hand.

The evaporator which is in direct contact with the upper flange is only used after the whole chamber has nearly reached a temperature of about 30°K. Otherwise one would produce thermal stresses which could be fatal for the window. During the cool-down period we observed maximum temperature differences of about 10°K over the upper flange.

Normally the chamber is filled with liquid hydrogen from a storage vessel. The liquid is filtered through a piece of milk filter. It is necessary to condense the last liters into the chamber, because the evaporation line leaves the chamber a little bit below the glass window. We mounted a condensing line, which is in thermal contact with the cooling system. Like in a counterflow heat exchanger the hydrogen gas is cooled by the gas stream coming from the evaporator and is condensed at 5 atm. Thus we have the alternative possibility to fill the chamber entirely by condensing.

In principle our chamber represents a closed and entirely filled liquid volume at working conditions. Temperature and pressure can be regulated by the amount of coolant which is allowed to evaporate. Two bellows valves which are operated by helium gas and placed on the upper flange serve as safety outlets when the pressure rises too much, see fig. 4.

In practice we found it convenient to regulate the chamber pressure independently from the temperature. The leakage through the bellows valve, which disconnects the condensing line from the chamber, amounts to some cm^3/s at a pressure difference of 1 atm. We pressurize the chamber liquid above its vapor pressure by applying a controlled pressure to the condensing line with the cold

bellows valve closed. The leakage transmits this overpressure to the chamber but does not influence the pressure drop during the 20 ms of expansion.

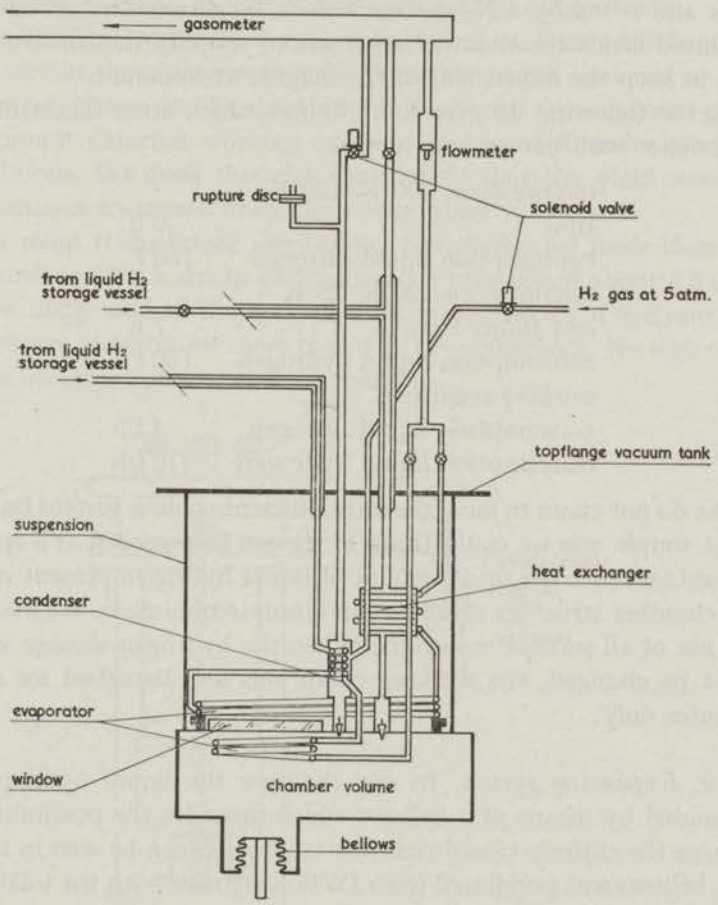

Fig. 5. The flow diagram. The right part of the chamber is far out of scale. The chamber is nearly symmetrical to an axis through the middle of the window as can be seen from fig. 4. The vacuum tank around the chamber is omitted.

At the beginning of a hydrogen run the temperature of the chamber has to be lowered as far as possible before liquid hydrogen is introduced into the cooling system. For this purpose we circulate liquid nitrogen through the evaporator inside the chamber until a mean temperature of about 120°K is reached.

A nitrogen cooled shield surrounds the whole chamber with the exception of the window side. It serves to lower the radiative heat input. The shield is placed in the high vacuum space of the vacuum tank and is fed by a N_2-storage vessel. No nitrogen reservoirs are mounted inside the chamber structure to simplify the construction and to keep the dimensions of the magnet at minimum.

In the following we give some figures which are a digest of the experience with our cooling system.

cooling down 300°K–120°K	
time	9 h
consumption liquid nitrogen	150 *l*
cooling down 120°K–25°K	
and filling time	7 h
consumption liquid hydrogen	150 *l*
working conditions	
consumption liquid nitrogen	4 *l*/h
consumption liquid hydrogen	10 *l*/h

We do not claim to have the most efficient cooling system but the most simple one we could think of. It can be regarded as a special advantage, that the total amount of liquid hydrogen present inside the chamber structure is kept at an absolute minimum. We avoided the use of all sorts of reservoirs. When the hydrogen storage vessel must be changed, the working conditions are disturbed for some minutes only.

§ 9. *Expansion system.* In our chamber the liquid hydrogen is expanded by means of a bellows which provides the possibility to enlarge the entirely closed chamber volume, as can be seen in fig. 4. The bellows was purchased from IWK Karlsruhe with the following specifications:

average cross-section	295 cm^2
material	tomback (80% Cu, 20% Zn)
number of convolutions	6
wall thickness	2 mm
maximum external working pressure	5 atm
maximum stroke	+11,4 mm; −5,7 mm
spring constant	220 kg/cm

From these numbers follows that the maximum change of volume is equal to 500 cm³. This means $\Delta V/V = 2.7\%$, as our total hydrogen volume amounts to 19 *l*. Experience showed that even a volume change of less than 1% at 27°K is sufficient to obtain tracks.

At 27°K hydrogen has a vapor pressure of ca. 5 atm. We kept the pressure in the chamber slightly above the vapor pressure so that no vapor phase could exist there. Consequently the above given maximum external working pressure is exceeded under working conditions. We took this risk considering that the yield strength of tomback increases when the temperature is lowered.

At room temperature our bellows has performed more than 10^4 expansions with a stroke of 6 mm and a pressure of about 4.5 atm. At ca. 30°K we had the bellows work with a stroke of 6–8 mm and a pressure of 6 atm for more than $1.5 \cdot 10^4$ expansions. No sign of an inelastic deformation has been found.

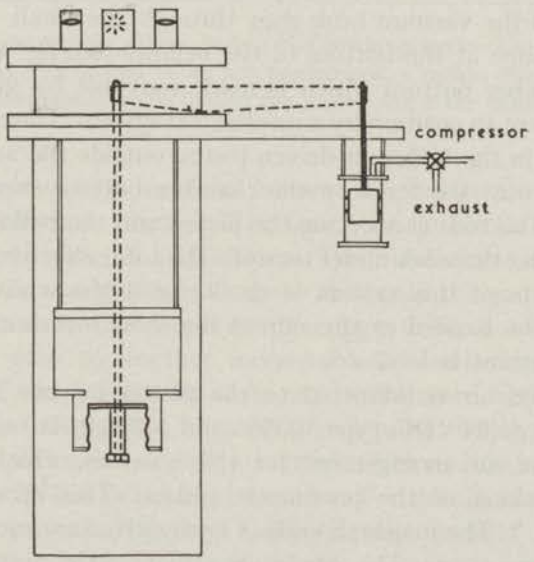

Fig. 6. The expansion system. The two rods and the double lever, which connect the bellows to the piston, are given by broken lines, because they are not cut by the section-plane.

It is advantageous to use a bellows with a large diameter if the chamber expands by its own pressure. The force F with which the

hydrogen acts on the movable chamber bottom becomes high and the needed stroke S small. The expansion time τ is diminished by both effects. The mass M of the mechanical system, however, increases with the cross-section of the bellows and consequently the expansion time τ lengthens again. Considering the three effects together the expansion time shortens if the bellows cross-section is enlarged. It is $\tau^2 = cMSF_{av}^{-1}$ which is roughly proportional to the inverse of the bellows cross-section. The dimensionless quantity c has a value $1.57 < c < 2$. F_{av} means the average force the liquid exerts on the expansion system during the time τ. With $M = 20$ kg, $S = 1$ cm and $F_{av} = 300$ cm^2. 2.5 atm we get $\tau = 7$ ms.

The connections between the chamber and the bellows are made by crimping, clamping and soft soldering in such a way that the soft soldering does not have to stand any stresses. As can be seen from fig. 4 no pressure shock can reach the vacuum tank in case of failure of the bellows. The connection between the space inside the bellows and the vacuum tank goes through the small hole in the soldered flange at the bottom of the bellows (see fig. 4 *u*).

The chamber bottom which is made movable by virtue of the bellows is kept in position by a mechanical system. The construction is sketched in fig. 6. An air driven piston outside the vacuum tank counterbalances the force on the chamber bottom exerted by the hydrogen. The rods connecting the piston and the bellows with the lever, transfer the work under tension. The total effective mass of all moving parts of this system is ca. 22 kg if the whole system is thought to be located at the side of the short leverarm. The ratio of the leverarms is 1 : 2.

Pressurized air is admitted to the piston by two Barksdale-3 way-$\frac{3}{4}$"-valves (24 VDC, type 103963 and 103964). It took us a long time to find an arrangement for these valves, which ensures a reliable working of the pneumatic system. This arrangement is given in fig. 7. The magnetic coils of both valves are energized until the expansion starts. The whole expansion cycle consists of four steps. The first two, 0–1 and 1–2, are responsible for expansion and recompression. The current in one of the valves is switched off each time. The last two steps serve to re-establish the begin condition: the current is switched on again without consequences for the pneumatic system. Without the constriction in the narrow line from the compressor to the second valve the pilot of the first valve

does not work properly at the fourth step 3–0. As switching element the germanium power transistor 2N268 is used, which is protected against voltage peaks V_{ec} higher than 33 V by the Zener power diode ZL33.

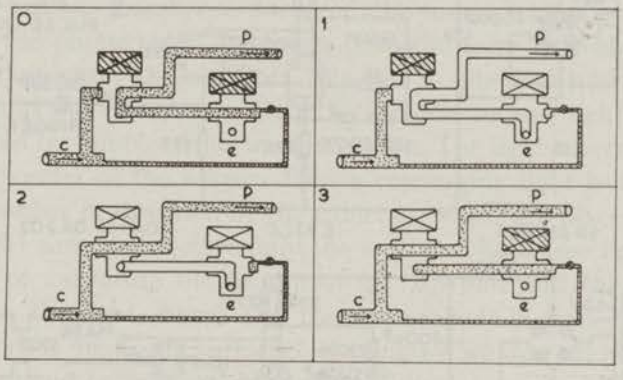

Fig. 7. The expansion valves during the working cycle. The hatched coils are energized, the dotted tubes are pressurized. *c* means the line from the compressor, *p* the line to the piston and *e* the exhaust.

The trigger system works as follows: the master pulse is fed into a monostable multivibrator. The time, the quasistable state lasts, is variable between 5 and 100 ms. The block pulse coming from this multivibrator passes a diode so that only the end of the pulse is transmitted. In this way a simple trigger delay is achieved. Next the signal goes to another monostable multivibrator. Here the duration of the quasistable state can be adjusted between 50 and 800 ms. The output is a negative block pulse, which undergoes a current amplification and sign inversion before it is sent onto the base of the 2N268 switching transistor. For details see fig. 8. Each Barksdale valve is triggered independently, so that the just described circuit is needed twice.

The time the bellows needs to perform an expansion of the chamber volume with a stroke of 6 mm is measured equal to 8 ms, if the chamber is at 6 atm. The total time of expansion and recompression can easily be varied by adjusting the independent delays of the Barksdale valves .We found a minimum duration of 20 ms, when the stroke is 6 mm, the chamber pressure 6 atm and

the piston pressure 9 atm. The limitation of expansion speed is given by the opening of the Barksdale valves. To minimize the

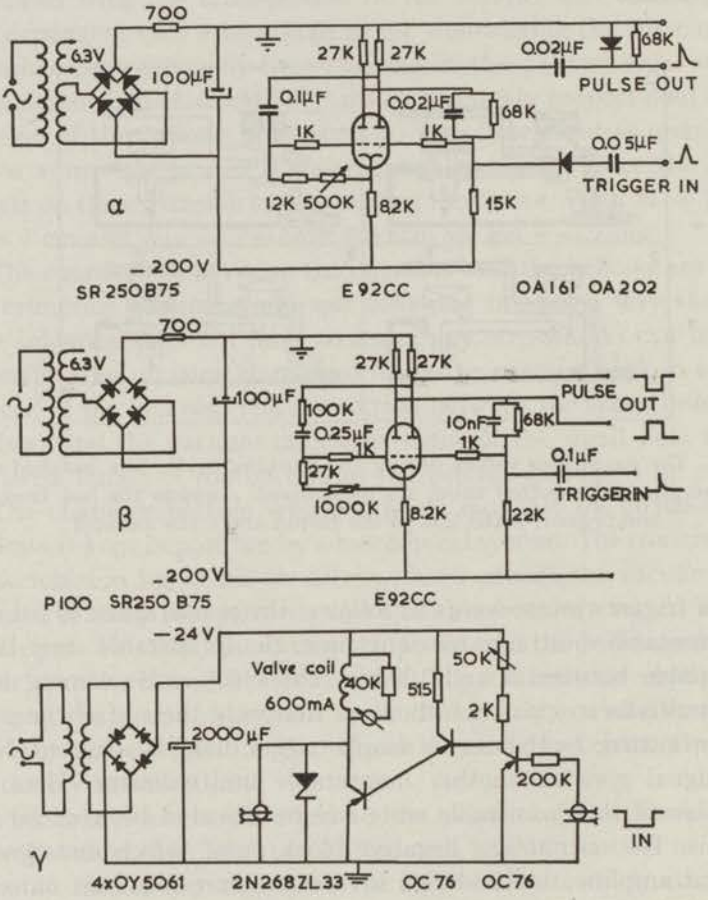

Fig. 8. Circuit of the expansion system. Each pulse-out serves as trigger for the subsequent unit. α effects an adjustable pulse delay and β forms the needed pulse shape for the switching unit γ.

time of expansion the exhaust line is connected to the space below the piston. Thus the piston receives the impact of the expanding air, which considerably reduces the time of expansion.

Chapter III

THE PHOTOGRAPHIC AND ILLUMINATION SYSTEMS.

§ 10. *Components of our optical system.* The whole construction of our bubble chamber is based on the use of an optical system, where the photographs are taken from the same side as the flash light illuminates the chamber. We put a spherical mirror at the bottom of our chamber so that the cameras receive light which is scattered by bubbles in forward direction. The light source is in the optical center of the mirror. Thus a converging light beam leaves the chamber in direction of the cameras, which are placed outside this light cone and receive only the scattered light (see fig. 3). The radius of curvature of the mirror is 1209 mm and the distance between the light source and the mirror is 1135 mm. The slight difference is due to the influence of the glass window and refraction by the liquid hydrogen, which cause a displacement of the optical center of the mirror.

The mirror itself is made from a brass plate, machined to spherical size, polished and covered with a chromium layer. Its surface is of minor quality as some scratches and pores are visible, but it has proved to give sufficient contrast.

The window was purchased from Schott in Mainz, Germany. It is made from tempered B.K.7 glass, 300 mm ⌀ and 35 mm thick.

The experience with the flash lamp will be described in § 13. Its actual position is not in the optical center of the mirror because we use a condensing system. An image of the light arc is formed in the optical center of the mirror. We call this image the effective light source.

The condensing system serves for different purposes, as will be described in § 12. It resembles an arrangement of optical components as normally used in lantern-slide projectors: there is a condenser (1 : 2), a "diapositive" and a projecting lens, the latter one placed where the condenser forms the effective light source. The diapositive is projected into a plane near the chamber. Besides other advantages this allows to have a sharply cut light cone in the neighborhood of the chamber in spite of the finite size of the light source. Thus the background is considerably improved.

We work with 3 cameras using unperforated 35 mm film. The objectives are placed on a circle with a diameter of 230 mm around

the effective light source. They have a focus of 100 mm and are used with a stop between 20 and 30. The actual demagnification is $m = 10$ regarding the image of the mirror on the film.

All glass parts of our optical system are coated, including the chamber window. Special care was taken to avoid reflection of the blue light which is predominantly emitted by the used flash lamp General Electric FT 230. About 1.4% is still reflected at each surface.

§ 11. *Bubble and source images.* In this section we will compare the amount of light a bubble scatters into a camera with how much parasitic light comes there by reflection at the window surfaces. The considerations are related to our illumination and photographic system, but they apply to other arrangements of the optical components, too.

The relative refractive index between liquid hydrogen and the vapor inside the bubbles at 27°K is ca. 1.10. Consequently light is scattered mainly in the forward direction. Usually the angular distribution of the scattered light is described by $I(\vartheta, r, R) = (r/R)^2 G(\vartheta)\ I_0$, where I_0 is the intensity of the incoming light at the position of the bubble, R is the distance at which $I(\vartheta, r, R)$ is measured and r is the radius of the bubble. I_0 is assumed to be constant throughout the chamber volume. $G(\vartheta)$ is the distribution function which contains all physical informations. It can be calculated using geometrical theory, see ref. [13]) and fig. 9. Conservation of light energy imposes the restriction on $G(\vartheta)$ that $\bar{G}^{\cos\vartheta} \leqslant \frac{1}{4}$. This follows from

$$I_0\, \pi r^2 \text{ (total incident light)} \geqslant \int_0^{\pi} I(\vartheta, r, R) \sin\vartheta\, 2\pi R^2\, \mathrm{d}\vartheta \text{ (total scattered light)}$$

G has the constant value of $\frac{1}{4}$ if all the light which falls on a bubble is isotropically scattered. One sees from fig. 9 how much $G(\vartheta)$ actually exceeds this average value for small ϑ.

Our cameras view the bubbles at an angle $\vartheta_0 = 5.8°$ from the direction of the unscattered light. The distribution function has the value $G(5.8) = 15$.

In the following we use the approximation of paraxial rays. For simplicity it is assumed that the distance between film and objective in our cameras equals the focal length f. The light which a bubble scatters into the iris of a camera amounts to $(r/R)^2 G(\vartheta_0)(f/F)^2 I_0 \pi/4$.

F is the stop number of the objective and R its distance from the bubble. This light is focussed into the area $\pi r^2(f/R)^2$ on the film. Consequently the bubble image receives the light per unit area $G(\vartheta_0)I_0/(4F^2)$.

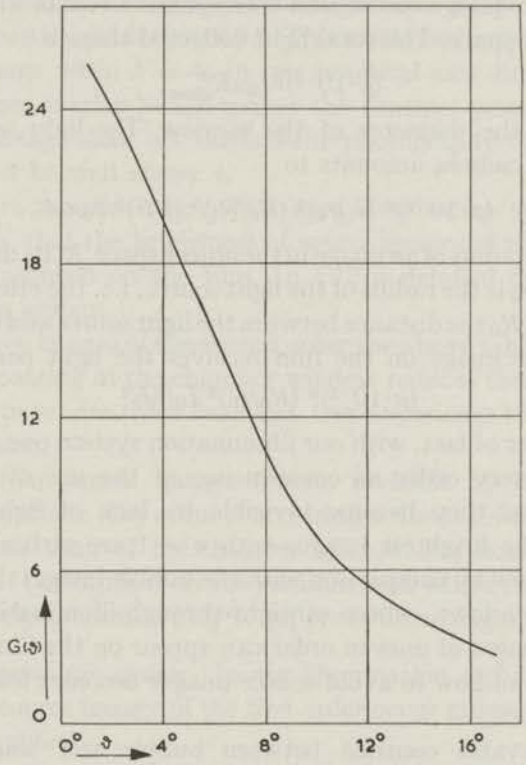

Fig. 9. Distribution function of light scattered by a spherical bubble in liquid hydrogen. The curve is calculated for $n_{rel} = 1.1$ [8]).

On the film appear images of the light source, too. These are due to single or multiple reflection of light at the window surfaces. In general they do not represent sharp images because they are out of focus. We will derive an expression for the amount of light focussed into these source images. First two definitions: We use the word parasitic when the effects of light reflection by the window are meant. For example, a parasitic source image is formed by light, which has undergone at least one parasitic reflection by the window. Furthermore, the order n of a source image indicates how many parasitic reflections have taken place before the image is formed.

At each parasitic reflection the intensity decreases as only $\rho\%$ are reflected. ρ equals 4 without coating and ca. 1 with single coating. If the flash light is filtered and double coating applied, ρ can be reduced to about 0.1.

To a source image on the film corresponds a real or virtual image in the object space. The total light collected there is

$$(\rho \cdot 10^{-2})^n I_0 \pi R^2_{\text{glass}} .$$

$2R_{\text{glass}}$ is the diameter of the window. The light sent through the iris of a camera amounts to

$$(\rho \cdot 10^{-2})^n \, (r_i/r_0)^2 \, (R_0/R_i)^2 \, (f/F)^2 \, I_0 \pi/4.$$

Here r_i is the radius of an image in the object space, R_i its distance from the camera, r_0 is the radius of the light source, i.e. the effective one in our case, and R_0 the distance between the light source and the window.

The source image on the film receives the light per unit area:

$$(\rho \cdot 10^{-2})^n \, (R_0/r_0)^2 \, I_0/4F^2.$$

As a matter of fact, with our illumination system one finds source images of every order as consequence of the use of a spherical mirror, unless they become invisible by lack of light intensity. Especially the brightest images with $n = 1$ are rather disturbing, as we will show by comparison with the bubble images. In chambers with two windows, where straight-through-illumination is used, no source images of uneven order can appear on the film. Therefore the question of how to avoid source images becomes less important in this case.

The achievable contrast between bubble and source images depends on the ratio k of the light per unit film area for both of them, $k = G(\vartheta_0)(\rho \cdot 10^{-2})^{-n} \, (r_0/R_0)^2$. This equation shows that k assumes a higher value for larger $G(\vartheta_0)$ i.e. smaller ϑ_0, and for larger r_0/R_0. Thus for the contrast between bubble and source images it is advantageous to photograph at small ϑ_0 and to illuminate the chamber by an extended light source.

Taking the actual values of our design, $R_0 = 90$ cm and $r_0 = 1.2$ cm we obtain:

$k = 6.7 \times 10^{-2}$ for $n = 1$ and $\rho = 4$ (uncoated)
$k = 2.7 \times 10^{-1}$ for $n = 1$ and $\rho = 1$ (coated)
$k = 1.7$ for $n = 2$ and $\rho = 4$ (uncoated)
$k = 27$ for $n = 2$ and $\rho = 1$ (coated) etc.

It is desirable to distinguish a bubble image even if it coincides with a source image. It would be better if one could keep the source image completely invisible. Therefore k should have as high a value as possible but definitely $\geqslant 4$ for all parasitic source images which appear on the film. For example the Agfa films Agepe and Agepan can be used with a gradation of 3.7. This would be enough to suppress a source image when $k = 4$. In our practical case however, some source images overlap which makes the contrast worse. Therefore if a source image shall not disturb the photography of bubbles its k-value must be well above 4.

It is a characteristic feature of the used illumination system in our construction, that the brightness of source images of the first order is strongly reduced on the film. In § 12 a detailed description is given of this system.

As to source images of the second order the above table of k-values shows that coating of the chamber window reduces their brightness sufficiently to render them harmless. Our experience has confirmed this conclusion.

Higher order source images remain invisible by lack of light intensity. But there may occur source images due to reflection at glass surfaces other than of the chamber window. For example coating and tilting of the window on the vacuum tank where the flash light enters has helped considerably to suppress disturbing source images.

§ 12. *Illumination system.* In our illumination and photographic system two source images of the first order occur unless some special tricks are applied.

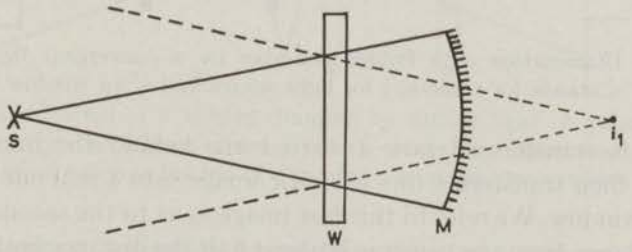

Fig. 10. The "first image" i_1 of the light source s. w means window and m mirror. Dashed lines indicate parasitic light, thin lines virtual light.

The first image is caused by a reflection of the incoming light at the window surface. A virtual 1 : 1 image is formed at twice the

distance "window-light source", which is seen by the cameras (see fig. 10). In fact this virtual image occurs twice as both surfaces of the window are reflecting.

The second image is also caused by a single parasitic reflection, but this time the spherical mirror is involved, as shown in fig. 11. The light is first reflected by the mirror, then by the window and finally by the mirror again before it falls into the irises of the cameras. Or in the language of geometrical optics: the mirror forms an image of the light source which coincidences with the light source itself; by intervention of a parasitic reflection at the window this

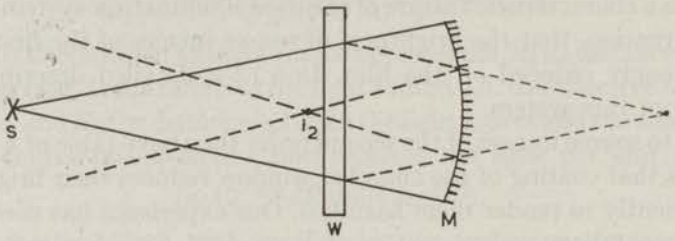

Fig. 11. The "second image" i_2 of the source s.

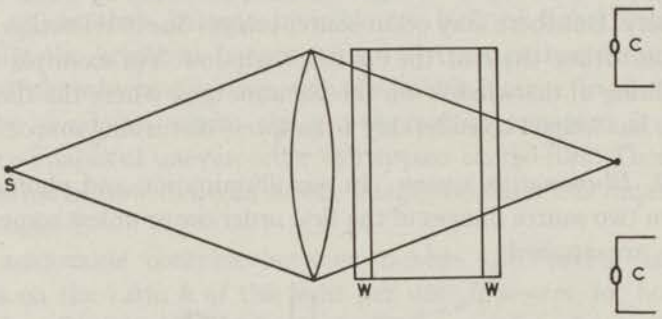

Fig. 12. Illumination of a bubble chamber by a convergent light beam. c stands for camera, s for light source and w for window.

image is transformed into a virtual one behind the mirror; the mirror then transforms this parasitic image into a real one in front of the window. We refer to this last image i_2 as to the second image. Its distance from the cameras is about half the distance between the first parasitic image and the cameras, and its size is about half the size of the light source. Therefore the cameras see both images equally bright and large. Again, the second parasitic source image occurs twice, as light is reflected at both sides of the window.

A way to avoid parasitic source images of the first order was proposed by Courant [14]). As an introduction we shall sketch two other illumination techniques used in bubble chamber work. In chambers with two vertical windows bubbles are normally photographed in a convergent light beam as shown in fig. 12. No source images of the first order appear on the film, only second order images whose brightness is reduced by coating the window.

Block *et al.*[4]) followed another method to obtain dark field illumination in their helium chamber. On one side of their chamber a diffuse light screen serves as a light source. A lens forms an image of the screen in a plane on the opposite side of the chamber where the cameras are placed. The relative positions of the screen, the lens, the chamber windows and the camera plane can be seen in fig. 13. The areas on the screen are blackened the images of which coincide with the irises of the cameras. Consequently no direct light falls into the cameras. There are still parasitic reflections, but because cameras and light source are on opposite sides of the chamber, only parasitic source images of the second and higher orders appear. They are barely visible on the film and cover a large area because an extended diffuse light source is used.

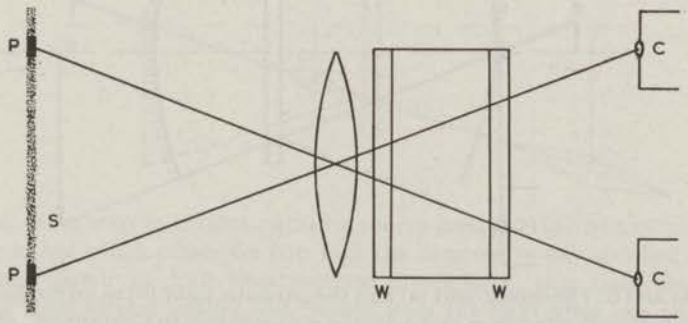

Fig. 13. Illumination of a bubble chamber by diffuse light. *p* indicates a black patch on the diffuse screen *s*, which serves as a light source. The image of *p* covers the iris of a camera *c*. *w* stands for window.

Now Courant proposes to combine these two systems in the following manner: 1. A pointlike source is used. By a condensing lens *co* its light is focussed into a real image *e* which is called the effective light source. A spherical mirror reprojects this effective source onto itself, as shown in fig. 14*a*. The cameras are arranged

on a circle around the effective source. 2. A diapositive *d* is located in the light beam immediately after it has left the condensing system. Its function can be understood from fig. 14*b*. A projecting lens *o* is placed where the effective source appears. The projected light which is reflected at the window surface, forms an image of the diapositive in the camera plane. Parasitic light of the first order is kept off the cameras *c*, if the areas on the diapositive, whose images coincide with the camera irises, are blackened.

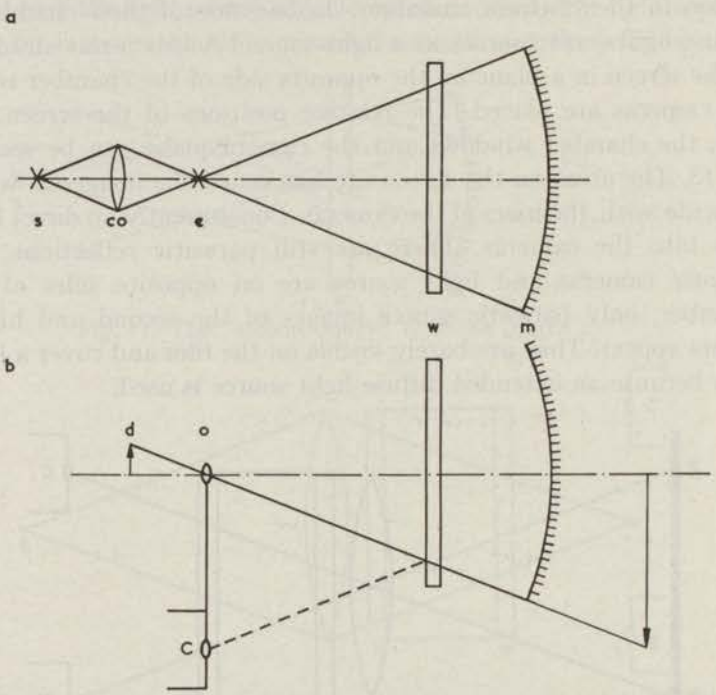

Fig. 14a and b. The direct light (a) and the parasitic light (b) in an illumination system with one window *w* and a mirror *m*, according to Courant [13]). *s* means light source; *d* the diapositive of which the projecting lens *o* forms an image in the plane of the camera *c*. This image is a parasitic one of the first order as indicated by the dashed line. *co* stands for collimator.

In other words, a spherical mirror hinders the entrance of parasitic light of zero order (direct light) into the cameras in analogy to the illumination method using a convergent light beam. The Block method simultaneously prevents the appearence of parasitic source images of the first order on the film.

We adapted the proposal of Courant in our illumination system. The use of a simple spherical mirror at the bottom of the chamber makes some modifications and precautions necessary, which will now be discussed. So far as we know we are the first who have brought the ideas of Courant into practice.

Courant assumes in his paper that a rectrograde reflector such as the Berkeley coat hanger system [6]) is used which casts back the direct light but absorbs all scattered and parasitic light, that falls on it. Therefore he only deals with the first source image, whereas in our case two source images occur. We must twice apply the trick of Courant to get rid of the second source image on the film, too. This is done by using a thick diapositive, bearing one set of black patches on either side. Following the path of the parasitic light, one set of them is projected onto the camera irises just as described above. The other set renders harmless the parasitic light, which forms the second source image in front of the chamber window.

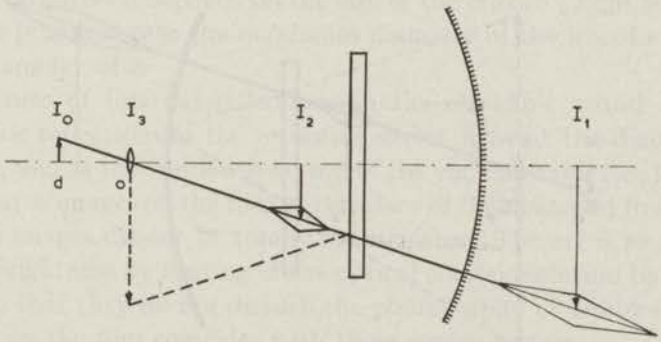

Fig. 15. First step to subdue parasitic source images. The light of the first source image which otherwise falls into the cameras, is extinguished by an absorbing patch I_0. Full lines indicate direct light, thin lines the light coming from virtual images and dashed lines the light after one parasitic reflection.

These facts are illustrated in figs. 15 and 16. The I_i and II_i represent one black patch or its images out of each set. The index $i = 0, 1, 2, 3$ denotes the plane in which I_i or II_i are situated. $i = 0$ is the plane of the diapositive, $i = 1$ and $i = 2$ the planes containing the first and the second source image respectively, and $i = 3$ the camera plane. The images of the black patches are surrounded by dark areas which resemble cigars. These are the regions where no direct

light comes as the consequence of the shadowing effect of the black patches. They should not extend into the chamber volume and render certain regions there unusable.

We first describe the sequence of images I_0–I_1–I_2–I_3 as shown in fig. 15. I_1 is an image of the black patch I_0 formed by the projecting lens *o*. This image is virtual, as no light penetrates the spherical mirror. A part of the light undergoes a parasitic reflection by the window and forms I_3, but most of the light is reflected by the spherical mirror which transforms the virtual image into the real image I_2. I_3 coincides with the iris of a camera, and this is the only intended result. Everything else is incidental and must not disturb the illumination. I_1 and I_2 are situated outside the chamber. Working with a small stop in the projecting objective *o* and a large enough light source we can keep the unilluminated regions around I_1 and I_2 out of the chamber, too. I_1 and I_2 stand for three images each as we work with three cameras and need one I_3 per camera iris.

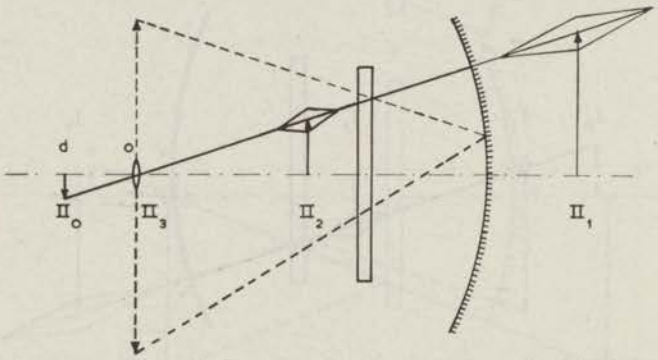

Fig. 16. Second step to subdue parasitic source images. The black patch II_0 absorbs the light of the second source image, which otherwise would fall into the cameras. Thin dashed lines mark the way of light from virtual parasitic source images, the other lines as in fig. 15.

Next we shall consider the sequence of the images II_0–II_1–II_2–II_3 as shown in fig. 16. Here II_2 is an image of II_0 formed by the objective *o*. Note that I_0 and II_0 lie on opposite surfaces of the ca. 15 mm thick diapositive. Therefore their images appear in very different planes. Now II_2 is transformed into the virtual image II_1 by the spherical mirror. Up to this point we only deal with the direct light, which is not seen by the cameras. The returning light, however, undergoes a parasitic reflection at the window. From II_1

this reflection forms a virtual image in the camera plane. The final step is that the spherical mirror produces the real image II_3 from the virtual one in the camera plane. II_3 is made to coincide with the iris of a camera. The consequence is that also the parasitic light which is successively reflected by the mirror, by the window, and by the mirror again, is kept off the cameras. II_1 and II_2 stand for the centers of three dark cigars each, so that in total there are twelve dark regions. All of them occur outside the chamber volume.

In practice the diapositive consists of a transparent polished lucite or glass window whereon arc segments are drawn with a pair of compasses, using black ink. These are the black patches mentioned above. Their right positions and thicknesses have been found by trial until the first order images of the light source on the films became nearly invisible.

The fact that a clear transparent diapositive is used instead of a diffuse one has the consequence, that the minimum effective stop of the objective *o* depends on the size of the effective light source *e*. In our practical case the maximum diameter of the iris of *o* equals the diameter of *e*.

Because of internal reflections in the objective *o* and due to parasitic reflections of the returning direct light at the diapositive *d*, at *o*, and at the window *p* on top of the vacuum tank (see fig. 17), the source images on the film at the place of the discussed first order source images cannot be totally extinguished. The art is to subdue their brightness by coating of the optical components and by tilting of *p* so that they do not disturb the photography of bubbles whose image on the film coincides with these source images.

For all details see the caption of fig. 17 which summarizes our actual design. In the drawing refraction effects in the glass windows and in the chamber liquid are omitted. In place of double images due to parasitic reflection at both window surfaces, simple images are drawn between the actual double images. When the lengths of the unilluminated regions were evaluated an enlargement due to this double occurrence was taken into account.

The diapositive plays another role as mentioned already. Because we work with an extended light source, it is impossible to have a sharply cut light cone projected into the chamber just by screening off the unwanted light with the help of an aperture between *e* and *p* (see fig. 17). We achieve homogeneous illumination of the chamber

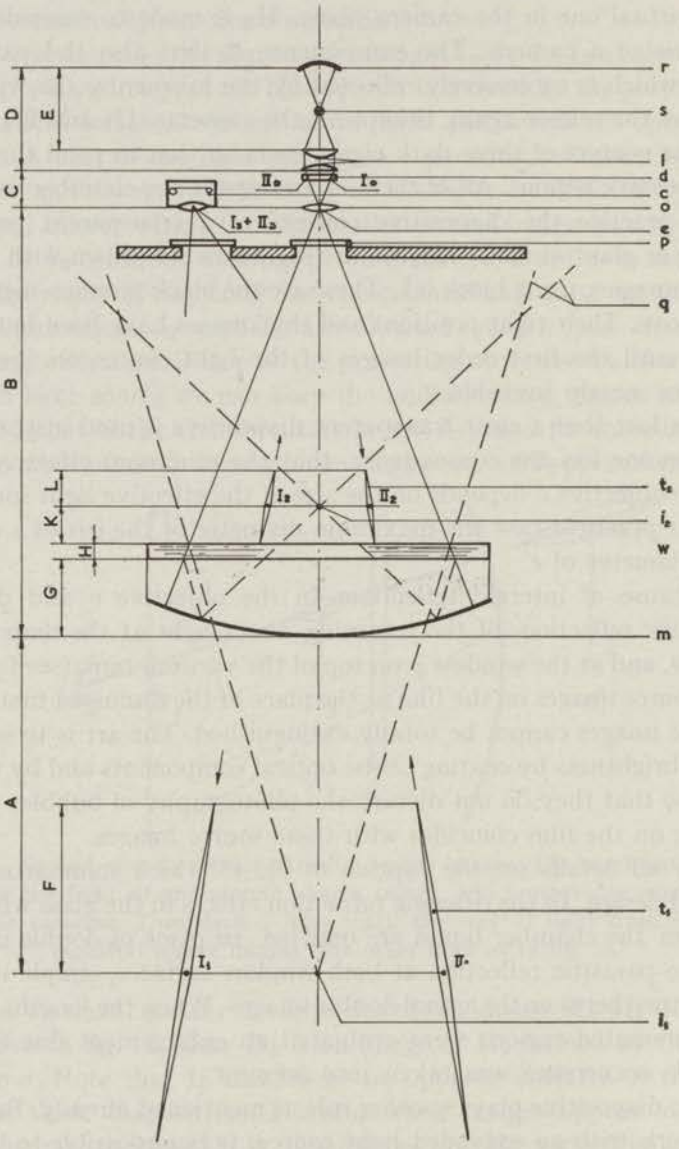
r
s
l
d
c
o
e
p
q
t_2
i_2
w
m
t_1
i_1
D
E
C
B
L
K
H
G
A
F
II_0
I_0
$I_2 + II_2$
I_2
II_2
I_1
IV_1

Fig. 17. General arrangement of optical components of the Leiden-chamber. All distances parallel to the optical axis are 1/20th of the true dimensions, whereas perpendicular to the axis this ratio is 3/20. Effects due to the refractive index of the glass windows and of liquid hydrogen are neglected in the drawing. These effects cause the I_1 and the II_1 as well as the I_2 and the II_2 to fall in slightly different planes. Note that I_1 and II_1 stand for three images each.

r reflector increasing the light efficiency; radius of curvature 59 mm, 54 mm ⌀.
s flash lamp, G.E. FT 230, maximum loading 200 J, ca 12 mm arc diameter.
l collimator, forming the 1 : 2 image *e*; two plane convex lenses of 47 mm ⌀, f = 118 mm and f = 60 mm.
d diapositive, ca. 15 mm thick, with three black patches on either side.
c camera. Boyer Aposaphir 1 : 10/100; used with a stop between 20 and 30; mounted on a Beatty film magazine. Three cameras are viewing the chamber, placed on a circle around *e* with 230 mm ⌀.
o projecting objective, Schneider Radionar 1 : 4.5/105.
e effective light source at the position of *o*.
p glass windows at room temperature, on top of the vacuum tank; the central one is tilted.
q cones of the parasitic light from the first and the second source image.
t_2 one of the six black tunnels (cigars) near the plane of the second image; the arrows on top of the cigars indicate, whether these regions of total shadow occur in the incident light (II_2) or in the light directed towards the cameras (I_2). Diameter amd length of these tunnels are 2.2 mm and 170 mm respectively. The length of tunnels is given taking into account reflection at both sides of the window. Actually two nearly coinciding tunnels are formed each time. Both of them fall inside the given t_i, i = 1,2.
i_2 second source image.
w chamber window, 35 mm thick, tempered BK 7 glass, 300 mm ⌀, coated.
m spherical mirror, radius of curvature 1209 mm, metallic.
t_1 one of the six virtual tunnels near the plane of the first source image.; diameter and length of these tunnels are 5 mm and 900 mm respectively.
i_1 first source image.

A = 770 mm	F = 450 mm
B = 1135 mm	G = 205 mm
C = 123 mm	H = 35 mm
D = 142.5 mm	K = 98 mm
E = 118 mm	L = 85 mm

without stray light outside the useful volume using the diapositive as aperture to limit the size of the light cone. This is possible because an image of this aperture is formed near the chamber.

§ 13. *Experiences with the flash lamp.* As a light source we use a General Electric FT 230. This lamp has the following specification:

design voltage	2 kV	electrode spacing	3.0–3.5 mm
minimum voltage	1 kV	filling gas	xenon
max. rating	200 J	flash duration ($\frac{1}{3}$ peak)	70 μs *)
trigger voltage	15 kV	flash rate	1/min *)
trigger energy	20 mJ	light colour	370mμ<λ<470 mμ *)
arc diameter	12 mm*)		

*) at maximum rating

Since a Hivolt-12 kV-unit and a thyratron 5C22 were at our disposal, we decided to design a trigger circuit utilizing these elements. The flash power is delivered by a Langham power unit working at 2200 V and 1450 V. The energy is stored in two TCC-Hiconol 33 μF capacitors which can be used in series or parallel or singly.

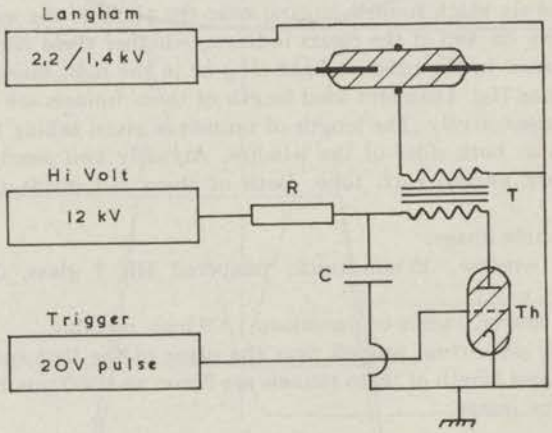

Fig. 18. The flash circuit. *Th* stands for thyratron, *C* for storage capacitor of the trigger pulse, *R* for the charging resistance and *T* for the pulse transformer.

The block scheme is given in fig. 18. The flash is started by a positive 20 V signal sent to the grid of the 5C22. It was not practicable to have a cathode follower as the last stage of the trigger unit, because

then the discharge in the 5C22 worked back with fatal consequence for the valves. The discharge of C (see fig. 18) via the thyratron causes a voltage drop of the plate which is transformed by T into a positive pulse and sent to the trigger electrode of the flash lamp. The 1 : 1 transformer T is homemade and consists of twice ten windings wrapped around ferroxcube discs 25 mm in diameter. TV-cable is used for the windings.

The trigger electrode of the flash lamp is a simple copper wire twined around the glass bulb. It is necessary to use a positive triggering pulse higher than 12 kV if the flash lamp is placed in the dark and incidental photoelectrons are absent.

The needed flash energy was determined by experiment. In our illumination system we use only about 6% of the light per flash. 50 joules per flash were sufficient when the diaphragm of the photographic objectives were stopped to F = 22 and the Adox film KB 17 was used.

The FT 230 is a lamp with a very narrow gap between the electrodes. Consequently the resistance during the discharge is considerably smaller than in normal flash lamps. We have determined the discharge resistance to be about $7 \cdot 10^{-2}$ ohms by measuring the damping of a LC-circuit in which the lamp formed the principle load. During the flash the stored energy is dissipated in the lamp and in the cables leading to it, in the ratio of the relative resistances. The needed cables have a length of some meters and conduct several thousand amperes in the short time the flash lasts. The copper cross-section must be at least 15 mm^2.

Acknowledgements. The basic design idea of the described bubble chamber arose from discussions between Prof. Dr. K. W. Taconis, Mr. E. S. Prins and one of the authors (J.R.). The stimulating interest and essential suggestions of Prof. Dr. K. W. Taconis throughout the whole work are gratefully acknowledged. The technical realization of the project has been mainly on hands of Mr. E. S. Prins of the Kamerlingh Onnes Laboratory.

This work was a part of the research program of the "Stichting voor Fundamenteel Onderzoek der Materie" (F.O.M.) and was made possible by financial support from the "Stichting voor Zuiver Wetenschappelijk Onderzoek" (Z.W.O.).

Received 18th August 1961

REFERENCES

1) Glaser, D. A., Phys. Rev. **87** (1952) 665 (L).
Glaser, D. A., Nuovo Cimento **11** suppl. 2 (1954) 361.
Glaser, D. A., Phys. Rev. **91** (1953) 762 (L).
Glaser, D. A., Handbuch der Physik, Springer, Berlin 1958, p. 314.
2) Seitz, F., Phys. Fluids **1** (1958) 2.
3) Goldburg, W. I., Phys. Fluids **1** (1958) 353.
4) Block, M. M., W. M. Fairbank, E. M. Harth, T. Kikuchi, C. Meltzer and J. Leitner, Proc. Int. Conf. on High Energy Accelerators and Instrumentation CERN 1959.
5) Eisler, F., R. Plano, A. Prodell, N. Samios, M. Schwartz, J. Steinberger, P. Bassi, V. Borelli, G. Puppi, H. Tanaka, P. Waloschek, V. Zoboli, M. Conversi, P. Franzini, I. Mannelli, R. Santangelo and V. Silvestrini, Nuovo Cimento **10** (1958) 468.
6) Chelton, D. B., D. B. Mann and R. A. Byrns, Proc. Cryogenic Eng. Conf., Boulder, 1956.
Gow, J. D. and A. H. Rosenfeld, Proc. Int. Conf. on High Energy Accelerators and Instrumentation CERN 1959.
7) CERN-report 4790/e.
8) Riddiford, L., H. B. van de Raay, N. C. Barford, C. C. Butler, D. McMullan, A. Thetford, D. B. Thomas, W. T. Welford, A. Amery, W. H. Evans, M. J. Moore, P. Polak, H. W. B. Skinner, P. R. Williams, D. Shaw, A. G. Ashburn and M. Snowden, Proc. Int. Conf. on High Energy Accelerators and Instrumentation CERN 1959.
9) Donaldson, R. and R. Watt, UCRL Eng. Note 4311–17/M19.
10) Budde, R., A. Burger, H. Filthuth, Y. Goldtschmidt-Clermont, H. M. Mayer, D. R. O. Morrison, Chr. Peyrou and J. Trembley, Nuovo Cimento **11** (1959) 778.
11) Derado, I., and N. Schmitz, Nuovo Cimento **11** (1959) 887.
12) Miner-Seastone, Handbook of Engineering Materials, John Wiley & Son, 1955, p. 4–145.
13) Davis, G. E., J.O.S.A. **45** (1955) 572.
14) Courant, H., Proc. Int. Conf. on High Energy Accelerators and Instrumentation CERN 1959.
15) Bradner, H., UCRL-report 9199 *).
16) Bugg, D. V., Progress in Nuclear Physics Vol. 7, Pergamon Press, London, 1959 *).

*) Recent general articles on bubble chambers, not cited in the text.

SAMENVATTING

Dit proefschrift bevat de beschrijving van een waterstof-bellenvat. Met behulp van een waterstof-bellenvat kan men eigenschappen en reacties van elementaire deeltjes bestuderen. Men schiet deze deeltjes in het met vloeibare waterstof gevulde vat. Wanneer men door expansie de druk in dit vat laat dalen, geraakt deze vloeistof in een oververhitte toestand, waardoor dampbellen gevormd worden en wel voornamelijk langs het spoor van de elementaire deeltjes, die zich op dat ogenblik door het vat bewegen. Deze bellensporen worden stereoscopisch gefotografeerd, waardoor de mogelijkheid ontstaat ze nader te bestuderen.

Met de bouw van het Leidse bellenvat werd begonnen in 1957 en het is verschillende malen getest. Het heeft een horizontaal venster aan de bovenzijde, waar doorheen de gebeurtenissen in het vat gefotografeerd kunnen worden. Aan de onderzijde bevindt zich een balg, met behulp waarvan het vat wordt geëxpandeerd. De horizontale diameter bedraagt 30 cm, het totale volumen is 19 *l* en het nuttig volumen is 14 *l*.

In hoofdstuk I wordt het bellenvat vanuit een algemeen gezichtspunt behandeld, waarmee de achtergrond gevormd wordt, waartegen de eigenschappen van ons bellenvat behoren te worden gezien. Achtereenvolgens worden besproken: de werking van het bellenvat in het algemeen; enige opmerkingen over bellenvorming; de eisen, waaraan een ontwerp voor een waterstof-bellenvat moet voldoen in verband met de belichting, de afdichtingen, het benodigde homogene magnetisch veld, het koelsysteem en het expansiemechanisme; de nauwkeurigheid van de bepaling van sporen en tenslotte de mogelijkheden van een waterstof-bellenvat.

Daarna wordt in hoofdstuk II een gedetailleerde beschrijving van ons bellenvat gegeven betreffende de algemene opzet, de constructie, het koelsysteem en het expansiesysteem. In het bijzonder geven wij in de eerste paragraaf een argumentering voor onze keuze van een vat met één venster.

Wegens zijn belangrijkheid en uitgebreidheid is de bespreking van het optische systeem apart ondergebracht in hoofdstuk III. Dit hoofdstuk bevat een algemene beschrijving van de samenstellende delen. Verder vergelijken wij het beeld van een dampbelletje met de verschillende spiegelbeelden van de lichtbron op de film. Er worden speciale voorzorgsmaatregelen besproken om deze spiegelbeelden te onderdrukken. Deze problemen hangen sterk samen met de bijzondere aard van het optische systeem in een bellenvat met één venster. Tenslotte rapporteren wij onze ervaringen betreffende de door ons gebruikte flitslamp en het bijbehorende elektrische circuit.

Electron tracks in the chamber. Each track gives an image-track at a vertical distance of about 2 cm. The 6 dark regions are out-of-focus images of the 6 black patches on the "diapositive", as described in section 12. The flares remain from the two first order images of the light source. The photograph is taken with a Ra-source at a distance of 30 cm from the center of the chamber. On the photograph the tracks are due to Compton electrons in the upper part of the chamber.

Teneinde te voldoen aan de wens van de Faculteit der Wis- en Natuurkunde volgt hier een overzicht van mijn universitaire studie.

Ik begon mijn studie in 1949 aan de universiteit te Göttingen en legde daar het „Vordiplom-Examen" in 1952 af.

Te Freiburg im Breisgau vervolgde ik mijn studie en deed in 1954 het „Diplom-Examen".

In hetzelfde jaar ging ik naar het Kamerlingh-Onnes Laboratorium, waar ik onder leiding van Prof. Dr. K. W. Taconis deelnam aan het onderzoek, dat Dr. D. H. N. Wansink verrichtte over stromingseigenschappen van vloeibaar ^3He–^4He mengsels. Tegelijkertijd voerde ik berekeningen uit over het fazenevenwicht van het twee-componenten-systeem H_2–O_2, H_2–N_2 en H_2–CO, hetgeen geschiedde in verband met de onderzoekingen van Dr. Z. Dokoupil in dit laboratorium.

Gedurende het jaar 1956 werkte ik in Italië, waar ik op verzoek van Prof. Dr. G. Careri deelnam aan de opbouw van het cryogene laboratorium te Frascati. In deze tijd voltooide ik tevens metingen betreffende de diffusie van ^3He in vloeibaar ^4He boven het λ-punt.

Vanaf maart 1957 ben ik in dienst van de stichting F.O.M. met de opdracht, onder leiding van Prof. Dr. K. W. Taconis een waterstof bellenvat te bouwen voor gebruik bij het synchrotron, dat te Delft in aanbouw is. Dit bellenvat is in mijn dissertatie beschreven. Bij dit werk werd ik geassisteerd door de heren D. Z. Toet en B. van Eijnsbergen, beiden nat. cand., door de heer J. Hemerik, gezel-instrumentmaker, en door volontairs van de HTS voor electronica Rens & Rens.

Leden van de technische staf van het Kamerlingh-Onnes Laboratorium waren betrokken bij het ontwerp en de konstruktie van het bellenvat; vooral de bijdragen van de heer E. S. Prins, leider van de konstruktie-werkplaats, zijn beslissend geweest voor het slagen van het hele project. Gedurende de proeven ontving ik veel hulp van de cryogene technici, in het bijzonder van de heer C. le Pair.

STELLINGEN

I

Bellenvorming langs de sporen van ioniserende deeltjes in oververhit vloeibaar helium II wordt bemoeilijkt door de grote warmtegeleiding van de vloeistof. Waarschijnlijk moet men de breekgrens van de vloeistof overschrijden voordat een effect optreedt.

Mendelssohn, K., Suppl. Nuovo Cimento **9** (1958) 227, discussie.

II

De wijze, waarop Fokker in zijn boek „Tijd en Ruimte, Traagheid en Zwaarte" de begrippen „interval" en „chronogeometrie" introduceert, kan aanleiding tot misverstand geven.

Fokker, A. D., Tijd en Ruimte, Traagheid en Zwaarte, De Haan N.V., Zeist 1960.

III

In Freon-bellenvaten neemt de bellendichtheid langs sporen van ioniserende, zeer snelle deeltjes toe met de kinetische energie van de deeltjes. Er werd tot nu toe geen invloed van de polariseerbaarheid van de vloeistof op de bellendichtheid, dus geen z.g. dichtheidseffect gevonden. Dit kan men verklaren door te veronderstellen, dat vooral ionisatie en excitatie van de binnenschillen van de vloeistofatomen voor bellenvorming verantwoordelijk zijn.

B. Hahn, E. Hugentobler, en F. Steinrisser, Proc. Conf. on Instrumentation for High Energy Physics, Berkeley 1960, 142.

IV

Chelton e.a. beweren, dat het rendement van koudeproductie bij 27°K een factor drie kan worden verbeterd, indien men niet slechts de verdampingswarmte van vloeibaar waterstof voor koeling benut, maar ook de koude van het waterstofgas, boven 27°K, nuttig gebruikt. Deze bewering is in zijn algemeenheid onjuist.

Chelton, D.B., J.W. Dean en B.W. Birmingham, Rev. Sci. Instr. **31** (1960) 712.

V

De gevonden verhoging van de vermoeiingssterkte van metalen in ultrahoge vacua maakt een onderzoek bij temperaturen beneden 25°K aantrekkelijk, omdat men in dit temperatuur-gebied gemakkelijk de vereiste zeer lage zuurstofdruk kan bereiken.

VI

Alles-Borelli e.a. vergelijken hun experimentele resultaten van de pion-proton-verstrooiing met het Lindenbaum-Sternheimer-model. Zij houden hierbij echter niet voldoende rekening met de mogelijkheid, dat interferentie kan optreden tussen de uittredende golven, die van de verschillende reactie-kanalen afkomstig zijn.

Alles-Borelli, V., S. Bergia E. Perez-Ferreira en P. Waloschek, Nuovo Cimento **14** (1959) 211.

VII

Gezien de resultaten van Gerritsen betreffende de ionisatie van vloeistoffen door alpha-deeltjes is het niet verwonderlijk, dat men in het Helium-bellenvat van de Duke-University geen verandering van de bellendichtheid langs de sporen van ioniserende deeltjes heeft kunnen vaststellen door aanbrengen van electrische velden tot een sterkte van 3 kV/cm. Helium is wél bijzonder geschikt voor een dergelijk onderzoek, indien men de electrische velden tot ca. 100 kV/cm zou kunnen opvoeren.

Gerritsen, A.N., Proefschrift Leiden 1948.

VIII

Shoenberg bespreekt in zijn boek „Superconductivity" de herkomst van de oppervlakte-energie, die in de grenslagen tussen de normale en supergeleidende gebieden aanwezig moet worden gedacht, en volgt daarbij de argumentatie van Pippard. De invloed van de indringing van een magnetisch veld wordt hierbij op een misleidende wijze behandeld.

Shoenberg, D., Super conductivity, Cambridge University Press 1952. Pippard, A. B., Proc. Camb. Phil. Soc. **47** (1951) 617.

IX

Een onderzoek, of en hoe de bellendichtheid langs de banen van ioniserende deeltjes in xenon-bellenvaten afhankelijk is van de hoeveelheid koolwaterstoffen, die men aan de vloeistof toevoegt, is van belang voor opheldering van de problemen t.a.v. de bellenvorming.

X

Bij metingen aan sporen in waterstof-bellenvaten vindt men, dat de minium-waarde van de bellendichtheid per lengte-eenheid pas bij aanzienlijk hogere energieën bereikt wordt dan men volgens de Bethe-Bloch-formule zou verwachten. Dit kan men verklaren door het feit, dat het z.g. dichtheidseffect t.g.v. de polariseerbaarheid van de vloeistof reeds een rol gaat spelen voordat het minimum bereikt wordt.

Peyrou, Chr., Proc. Conf. on Instrumentation for High Energy Physics, Berkeley 1960, 157.

XI

In vertalingen uit het nederlands in het duits of bij citaten van duitse teksten vindt men vaak de foutieve schrijfwijze sz i.p.v. ss (β); zie bijvoorbeeld de eindexamenopgaven voor middelbare scholen 1961.
Deze schrijfwijze berust op een misverstand.